Title

Intense formation of secondary ultrafine particles from Amazonian vegetation fires and their invigoration of deep clouds and precipitation

Journal

One Earth, 7(6)

ISSN

2590-3330

Authors

Shrivastava, Manish

Fan, Jiwen

Zhang, Yuwei

et al.

Publication Date

2024-06-01

DOI

10.1016/j.oneear.2024.05.015

One Earth

Article

Intense formation of secondary ultrafine particles from Amazonian vegetation fires and their invigoration of deep clouds and precipitation

Graphical abstract

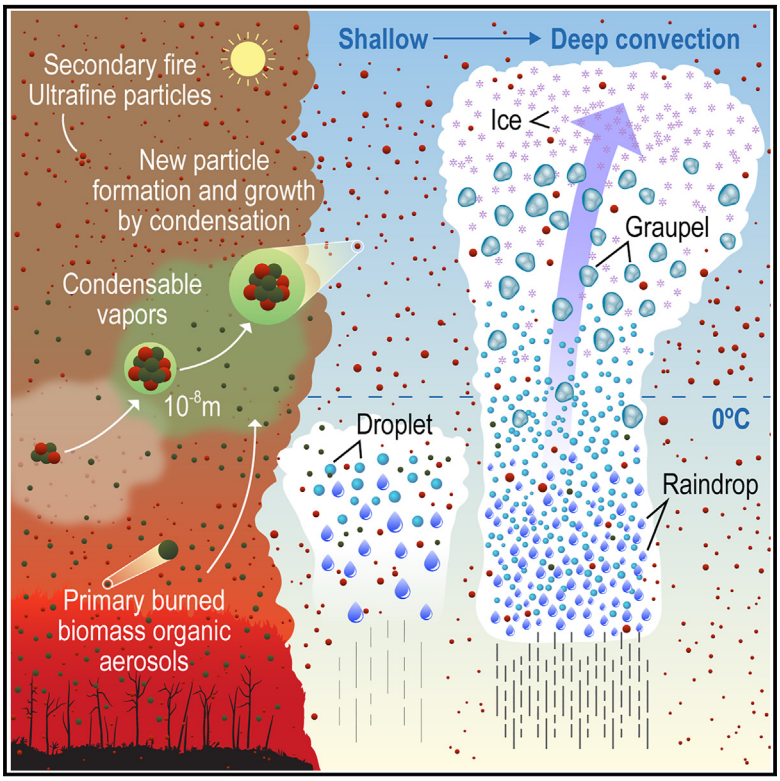

Authors

Manish Shrivastava, Jiwen Fan, Yuwei Zhang, ..., Neil M. Donahue, Yuan Wang, John H. Seinfeld

Correspondence

manishkumar.shrivastava@pnnl.gov (M.S.),
fanj@anl.gov (J.F.)

In brief

Ultrafine particles (UFPs) in biomass-burning smoke are formed by efficient nucleation mechanisms, including dimethylamines and sulfuric acid, and nucleated clusters grow by the condensation of oxidized organic vapors. UFPs may cause a stronger storm with a larger anvil and heavier rain, while larger particles directly emitted by fires delay and suppress rain.

Highlights

- Aircraft measurements in vegetation fires show abundant ultrafine particles (UFPs)
- Previous model formulations greatly underpredict the observed fire UFPs
- Nucleation of dimethylamines from fires with sulfuric acid explains observed UFPs
- UFPs from fires intensify deep convective clouds and precipitation

Shrivastava et al., 2024, One Earth 7, 1029–1043
June 21, 2024
https://doi.org/10.1016/j.oneear.2024.05.015

CellPress

One Earth

CellPress
OPEN ACCESS

Article

Intense formation of secondary ultrafine particles from Amazonian vegetation fires and their invigoration of deep clouds and precipitation

Manish Shrivastava,[1,17,*] Jiwen Fan,[2,*] Yuwei Zhang,[1] Quazi Z. Rasool,[1,15] Bin Zhao,[3] Jiewen Shen,[4] Jeffrey R. Pierce,[5] Shantanu H. Jathar,[6] Ali Akherati,[6,16] Jie Zhang,[1] Rahul A. Zaveri,[1] Brian Gaudet,[1] Ying Liu,[1] Meinrat O. Andreae,[7,8,9] Mira L. Pöhlker,[10,11] Neil M. Donahue,[12] Yuan Wang,[13] and John H. Seinfeld[14]

[1]Pacific Northwest National Laboratory, Richland, WA 993522, USA
[2]Argonne National Laboratory, Lemont, IL 60439, USA
[3]State Key Joint Laboratory of Environmental Simulation and Pollution Control, School of Environment, Tsinghua University, Beijing 100084, China
[4]State Environmental Protection Key Laboratory of Sources and Control of Air Pollution Complex, Beijing 100084, China
[5]Department of Atmospheric Science, Colorado State University, Fort Collins, CO 80523, USA
[6]Mechanical Engineering, Colorado State University, Fort Collins, CO 80523, USA
[7]Max Planck Institute for Chemistry, 55128 Mainz, Germany
[8]Scripps Institution of Oceanography, University of California, San Diego, La Jolla, CA 92037, USA
[9]Department of Geology and Geophysics, King Saud University, Riyadh 11451, Saudi Arabia
[10]Atmospheric Microphysics Department, Leibniz Institute for Tropospheric Research, 04318 Leipzig, Germany
[11]Faculty of Physics and Earth Sciences, Leipzig Institute for Meteorology, University of Leipzig, 04103 Leipzig, Germany
[12]Center for Atmospheric Particle Studies, Carnegie Mellon University, Pittsburgh, PA 15213, USA
[13]Department of Earth System Science, Stanford University, Stanford, CA 94304, USA
[14]Division of Chemistry and Chemical Engineering, California Institute of Technology, Pasadena, CA, USA
[15]Present address: Cooperative Institute for Research in Environmental Sciences (CIRES), University of Colorado, Boulder, CO, USA and NOAA Chemical Sciences Laboratory (CSL), Boulder, CO, USA
[16]Present address: Ramboll USA, San Francisco, CA, USA
[17]Lead contact
*Correspondence: manishkumar.shrivastava@pnnl.gov (M.S.), fanj@anl.gov (J.F.)
https://doi.org/10.1016/j.oneear.2024.05.015

SCIENCE FOR SOCIETY Fine particles in wildfire smoke can lower air quality and harm human health. Smoke can also influence weather and climate by modifying cloud formation and changing how much of the sun's energy is reflected or absorbed by the atmosphere. Compared to larger particles directly emitted from fires, the formation and presence of ultrafine particles (UFPs) have previously been overlooked, as it was thought that they were quickly "scavenged" by the larger particles. However, we found that UFPs were abundant in aircraft measurements of smoke from vegetation fires in the Amazon, and their formation and survival were favored. Furthermore, high-resolution modeling showed that these UFPs may intensify cloud convection and heavy rain. This research deepens our understanding of how vegetation fires impact weather and climate change.

SUMMARY

New particle formation (NPF) in fire smoke is thought to be unlikely due to large condensation and coagulation sinks that scavenge molecular clusters. We analyze aircraft measurements over the Amazon and find that fires significantly enhance NPF and ultrafine particle (UFP < 50 nm diameter) numbers compared to background conditions, contrary to previous understanding. We identify that the nucleation of dimethylamine with sulfuric acid, which is aided by the formation of extremely low volatility organics in biomass-burning smoke, can overcome the large condensation and coagulation sinks and explain aircraft observations. We show that freshly formed clusters rapidly grow to UFP sizes through biomass-burning secondary organic aerosol formation, leading to a 10-fold increase in UFP number concentrations. We find a contrasting effect of UFPs on deep convective clouds compared to the larger particles from primary emissions for the case investigated here. UFPs intensify the deep convective clouds and precipitation due to increased condensational heating, while larger particles delay and reduce precipitation.

INTRODUCTION

Aerosols influence climate forcing by scattering and absorbing radiant energy and by acting as cloud condensation nuclei (CCN) and ice nuclei particles, thereby affecting clouds and precipitation. Aerosol interactions with radiation and clouds constitute one of the largest uncertainties in climate forcing.[1,2] Biomass burning is a major source of directly emitted (primary) aerosol particles globally, accounting for ~42% and 74% of global black carbon and primary organic aerosol (POA) by mass, respectively.[3] Aerosols from biomass burning have been found to affect severe hazardous weather, heavy precipitation and hail,[4] air quality, atmospheric composition, clouds and precipitation,[5] and human health.[6,7] In a future warming climate, with the expected increases in frequencies of extreme climate events including exacerbating wildfires in the Amazon and worldwide, biomass-burning aerosols and their effects on weather and climate will become increasingly important.[8,9]

New particle formation (NPF) is the major source of atmospheric particle number concentrations in many regions around the world. NPF occurs when gaseous precursor molecules combine into stable clusters; once formed, these clusters can grow further and function as CCN.[10] Laboratory measurements have demonstrated evidence of nucleation in biomass-burning plumes that could provide large sources of CCN in the atmosphere.[11] In addition, aircraft-based field measurements of biomass-burning plumes in different regions have provided evidence for NPF, for example, within fresh daytime wildfire plumes in South Africa[12,13] and aged biomass-burning plumes over boreal forests and the western United States.[14–16] Biomass burning is widely used for land clearing and agricultural expansion, infrastructure development, and mining over the Amazon rainforest.[17] To the best of our knowledge, nucleation in biomass-burning plumes over tropical forests such as the Amazon has not been reported previously, likely due to the lack of relevant measurements of particle size distributions (SDs) within plumes. Furthermore, the mechanisms responsible for the nucleation and formation of ultrafine particles (UFPs, with sizes <50 nm diameter) within wildfire plumes are not well understood. While accumulation-mode and coarse-mode particles can be easily activated to form cloud droplets, UFPs are conventionally thought to make a negligible contribution to droplet nucleation due to the high supersaturations (SSs) required for their activation. However, UFPs could be activated in strong updrafts of deep convective clouds that can have high water vapor SSs in the Amazon.[18] Recent observations suggest that particles as small as 25–30 nm in diameter (in the UFP range) could serve as CCN and activate to cloud droplets within marine stratus clouds over oceans with SSs > 0.5%.[19] UFPs can also grow from secondary processes or cooling and condensation of semivolatile species. Due to their large number concentrations, UFPs have the potential to greatly modify cloud properties.

Long-term observations over the Amazon rainforest show that biomass burning during the dry season from August to November is associated with increased CCN and accumulation-mode particles and high organic mass fractions (~90%).[20] Owing to their emissions of numerous accumulation- and coarse-mode particles, fire plumes have large condensation sinks (CSs). CSs are the first-order loss rate due to the condensation of low volatility vapors on particles and are primarily governed by the preexisting particle number SD. CSs could limit new NPF by scavenging the vapors needed for nucleation and growth.[21–23] However, fires also emit large amounts of precursor gases such as ammonia (NH_3), amines that include dimethylamines (DMAs) important for nucleation,[24,25] sulfur dioxide (SO_2), and organic vapors,[26,27] including low-volatility and extremely-low-volatility organics (ELVOCs).[27,28] ELVOCs can be defined as organic gases with saturation vapor concentrations $C^* \leq 3 \times 10^{-5}$ μg m^{-3} and can promote nucleation and growth of molecular clusters due to their low volatility.[29,30] To maintain high nucleation rates, the sources (emissions and chemical production rates) of these precursors need to increase with their CSs (proportional to the particle SDs in smoke). The oxidation of SO_2 and organic vapors by oxidants such as hydroxyl radicals generates sulfuric acid and lower volatility organics that undergo multiphase chemistry causing NPF and growth.[2,10,31,32] Previously, 7 different nucleation mechanisms were included in the Weather Research and Forecasting model coupled with Chemistry (WRF-Chem).[33] They were shown to successfully predict NPF within the background Amazon and within the urban Manaus, Brazil plume over the Amazon.[34] However, we found in this work that these mechanisms greatly underpredict the observed UFP SDs within vegetation fire-affected airmasses in the Amazon, representing a key knowledge gap in our understanding of NPF mechanisms. To address this gap, we incorporated our best knowledge of another efficient nucleation mechanism—the DMA + sulfuric acid (H_2SO_4) mechanism, which has previously been evaluated with urban field measurements in China.[35] Although the DMA + H_2SO_4 mechanism has not been previously reported as a key nucleation mechanism in biomass-burning smoke, we show that it is needed to explain UFP concentrations observed by the aircraft in vegetation fires over the Amazon. We note that DMA emissions sources (needed for nucleation) from biomass-burning fires are not included in previous models, which limits their ability to predict nucleation in biomass-burning-affected airmasses. Biomass burning is one of the main natural sources of DMA emissions.[25]

In this study, we analyze aircraft measurements of particle SDs above the Amazon during two field campaigns over the Amazon: the Green Ocean Amazon (GoAmazon 2014/5)[36] and the Aerosol, Cloud, Precipitation, and Radiation Interaction and Dynamics of Convective Cloud Systems-Cloud Processes of the Main Precipitation Systems in Brazil: A Contribution to Cloud Resolving Modeling and to the GPM (Global Precipitation Measurement) (ACRIDICON-CHUVA),[37] and show that NPF in vegetation fires in the Amazon increases UFP number concentrations by more than an order of magnitude compared to the background. In contrast, previous understanding suggests that nucleated particles in biomass-burning smoke might be quickly lost by coagulation to preexisting primary biomass-burning aerosols. Using detailed regional modeling, we elucidate the key mechanisms governing nucleation in fire-affected airmasses. To predict the effects of the DMA + H_2SO_4 nucleation mechanism within fires on UFPs, we include the biomass-burning emissions' source of DMA within a detailed regional model as described in the experimental procedures section DMA emissions in biomass-burning fires. The sinks of DMA include their chemical loss by gas-phase

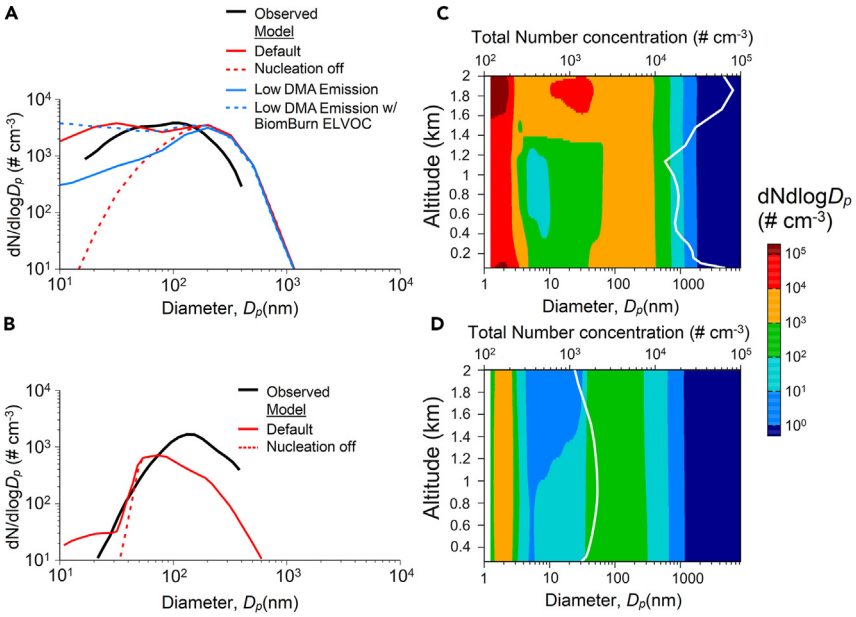

Figure 1. DOE G-1 aircraft-based FIMS-measured (black) and WRF-Chem-model-predicted particle number SD statistics

Data are shown at altitudes <2 km during the daytime on September 30, 2014, a representative day for biomass burning.

(A and B) Fire-affected airmasses (A) and the background Amazon (B). For the measurements onboard the aircraft, fire-influenced airmasses are determined based on the biomass-burning tracer acetonitrile (*m/z* 42 > 0.4 ppb) measured by PTR-MS. To select fire-influenced airmasses in the WRF-Chem results, predicted number SDs are averaged over the top 5th percentile of primary BBOA concentrations (the 95th–100th percentiles) calculated over the same latitude, longitude, altitude, and time ranges sampled by the aircraft to represent relatively fresh fire-affected airmasses. The red solid lines in (A) and (B) correspond to the default WRF-Chem simulation, which includes all 8 nucleation mechanisms, the red dashed line corresponds to model simulation with nucleation off, the solid blue line represents a simulation with the lower bound of DMA emissions from biomass burning, and the blue dashed line corresponds to WRF-Chem predictions with the lower bound of DMA emissions but includes a source of ELVOCs (upper bound) from biomass burning (biomburn ELVOC), as described in the text.

(C and D) Colored contours in (C, biomass-burning fires) and (D, background) represent WRF-Chem-predicted variations of particle SDs as a function of height above ground level at 0- to 2-km altitudes averaged over the regions sampled by the G-1 aircraft. The white lines on (C) and (D) are the WRF-Chem-simulated total particle number concentrations indicated on the top x axes.

reaction with OH radicals, and the irreversible uptake of DMA by preexisting aerosols. Moreover, for a typical shallow-to-deep convection cloud case in the dry season over the Amazon, we show that UFPs may increase deep convective cloud intensity, cloud fraction, and precipitation. These results provide important insights into aerosol-cloud interactions from secondary ultrafine biomass-burning aerosols.

RESULTS

Methods summary

By analyzing aircraft observations and conducting high-resolution regional WRF-Chem version 4.2 model simulations, we investigate the statistical properties of airmasses affected by vegetation fire smoke and how smoke changes particle SDs compared to relatively cleaner regional background airmasses. The fire-affected aerosols in this study represent near-plume conditions for small vegetation fires. We conduct simulations with two detailed modeling formulations integrating the latest mechanistic understanding of NPF, secondary organic aerosol (SOA) chemistry, and cloud microphysics: (1) the detailed NPF and SOA chemistry processes represented in regional WRF-Chem simulations at 10-km grid spacings covering a domain of 1,500 × 1,000 km centered at the Manaus urban area in the Amazon (Figure S1; Table S1), and (2) WRF coupled with the spectral-bin microphysics (WRF-SBM) model[38,39] for simulating impacts of biomass-burning aerosols on clouds and precipitation. Aerosol SD, vertical profile, and hygroscopicity for particles within fire-influenced airmasses and the background Amazon are derived from the WRF-Chem simulations and then fed to the WRF-SBM model. We evaluate predictions of size-resolved aerosol number concentrations with aircraft-based field measurements and precipitation properties with S-band radar data. The WRF-Chem model configuration used to model NPF, UFPs, and SOAs in our study is described in detail in the experimental procedures and the supplemental experimental procedures.

Our "default" WRF-Chem simulation includes all 7 nucleation mechanisms previously applied to the Amazon.[33] Additionally, it includes the DMA + H_2SO_4 nucleation mechanism and detailed treatments of NPF and growth, SOA formation, and ELVOCs from monoterpene oxidation represented by the radical two-dimensional volatility basis set (R2D-VBS),[33,34] as described in the experimental procedures section biogenic monoterpene ELVOCs. Biomass-burning SOA (BBSOA) formation is a key contributor to NPF in fire-affected airmasses and is simulated by a novel parameterization described in the experimental procedures section simulating BBSOA from VOC oxidation. However, the default WRF-Chem simulation excludes ELVOCs that are formed by the oxidation of organic vapors emitted in vegetation fire smoke. To assess the effects of uncertainty in DMA emissions from fires and the likely role of ELVOCs formed by the oxidation of biomass-burning organic vapors on UFP number concentrations, we conduct additional WRF-Chem sensitivity simulations as described in results and Note S1. We also assess the role of nucleation in predicting UFPs within fire smoke by turning nucleation off in the model as another sensitivity simulation.

Most of the results presented here focus on September 30, 2014, since measurements identified this day as the clearest case for vegetation fire aerosols that evolve with a typical case of clouds transitioning from shallow to deep convection, but

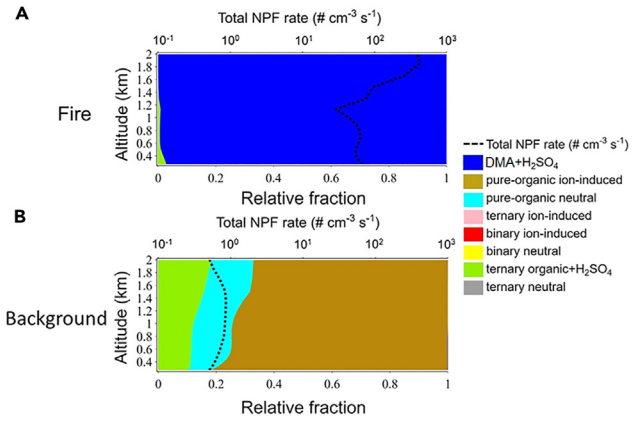

Figure 2. Relative contribution of the 8 different nucleation mechanisms to NPF rates predicted by WRF-Chem

Data are shown as a function of height above ground level at 0- to 2-km altitude during the daytime over the Amazon on September 30, 2014.

(A and B) Vegetation fire-influenced airmasses (A) and the background Amazon (B). The black dashed line on the panels represents the total NPF rate indicated on the top x axes.

vegetation fires occurred on other days as well (e.g., September 25, 2014).

G-1 aircraft-measured and WRF-Chem-predicted particles

Figure 1 compares aircraft-based fire-influenced and background measurements of particle SDs (ranging from 15 to 400 nm in diameter) using a fast integrated mobility spectrometer (FIMS) instrument on a representative biomass-burning day (September 30, 2014). Measured UFP number concentrations are ~1–2 orders of magnitude higher within fire-affected airmasses compared to the background (black lines in Figure 1A vs. Figure 1B). The default WRF-Chem simulations include the DMA + H_2SO_4 nucleation mechanism described earlier (solid red line, Figure 1A) and predict the large observed enhancement of UFP number within fires compared to the background (Figure 1B). Since CS is primarily governed by the preexisting particle number SD,[21–23] the agreement of the particle number SD simulated by WRF-Chem with the measured particle number SD (Figure 1A, red vs. black solid lines) implies an agreement of the modeled CS with measurements.

Figures 1A and S2 assess the sensitivity of WRF-Chem predictions to the definitions of fire-affected airmasses in the model. WRF-Chem simulations averaged over the top 5th percentile of the simulated directly emitted primary biomass-burning organic aerosol (BBOA) are denoted by the solid red line in Figure 1A in the same region sampled by the aircraft. These averaged number concentrations (over the top 5th percentile of BBOA) of ~4,000 cm^{-3} agree with aircraft-measured concentrations of ~3,300 cm^{-3}, while the corresponding WRF-Chem simulated particle number concentrations averaged over the top 50th percentile of BBOA (red solid line in Figure S2) are lower at ~1,800 cm^{-3}. However, the fractions of particle numbers between 10 and 100 nm are predicted as ~60% with both of the definitions of fire-affected airmasses (using the top 5th and 50th percentile BBOA criteria) and are in good agreement with the aircraft-measured fraction of ~60%. Turning off nucleation in WRF-Chem (dashed red line, Figure 1A) causes the model to underestimate UFP number concentrations by approximately an order of magnitude compared to observations and decreases the simulated fraction of 10- to 100-nm-diameter particle numbers to 20% (the observed fraction is 60%). The simulations indicate that fires are widespread over the Amazon and increase UFPs by an order of magnitude compared to the background near the surface (Figures 1C, 1D, and S3, top panels), as well as increase CCN (at 0.5% SS) by up to 200% (Figure S3, bottom panels). The simulation including nucleation shows a large increase in particle number within the ultrafine and accumulation-mode size range in fire-affected airmasses compared to the Amazonian background (Figures 1C and 1D) at 0- to 2-km altitudes. Although the greatest increase in particle number within fire-influenced regions compared to the background (Figure 1C vs. Figure 1D) corresponds to the nucleation mode (1–3 nm), the growth of these newly formed particles to larger sizes causes substantial increases in particle number within fire-affected airmasses (Figures 1C and 1D), especially over the particle size range <100 nm diameter measured by FIMS.

Although the 8th nucleation mechanism (DMA +H_2SO_4) has not been previously implemented and evaluated in biomass-burning smoke, we find that this mechanism predominates within fire-affected airmasses (Figure 2A), with a simulated total nucleation rate of ~100–700 cm^{-3} s^{-1} (dashed black line, Figure 2A). In contrast, simulated nucleation rates (<1 particle cm^{-3} s^{-1}, dashed black line in Figure 2B) over the background Amazon are at least two orders of magnitude smaller compared to fire-influenced airmasses. Pure organic ion-induced nucleation is the dominant contributor to these small nucleation rates over the background Amazon (Figure 2B), with pure organic neutral and ternary organic + H_2SO_4 as other contributing mechanisms. This is consistent with the understanding that the background Amazon lacks NPF near the surface, most likely due to the lack of SO_2 sources needed to form H_2SO_4 that is key for nucleation.[40] In addition, the high near-surface temperatures over the Amazon reduce organic-mediated nucleation rates near the surface compared to the upper troposphere.[33]

WRF-Chem-simulated DMA concentrations vary over a range of 1–10 pptv in fire-affected airmasses as shown in Figure S4A, in agreement with the ranges of DMA concentrations measured in other polluted urban locations.[35,41] In addition to DMA, H_2SO_4 is important for nucleation, and the simulated gas-phase H_2SO_4 agrees well with measurements at the T3 site (over the Manaus urban area) using a chemical ionization mass spectrometry instrument, the only available H_2SO_4 measurements during the field campaign (Figure S4D). As described in the experimental procedures section compensating CSs with smoke sources of nucleating species, chemical production/emission rates of nucleating vapors in smoke need to be proportional to their loss rates (represented by CSs) in smoke so that sufficiently high pseudo-steady-state concentrations of nucleating vapors are maintained to explain the UFP concentrations observed by the aircraft.

Effects of variability in DMA emissions on UFP numbers

DMA emissions from fires exhibit substantial variability and are estimated based on their reported ratios to NH_3 within wildfire plumes based on Ge et al..[24] Although within the default

WRF-Chem simulation we used an average DMA to NH_3 emissions ratio of 0.017 from fires based on Ge et al.,[24] we assessed the impact of the variability in DMA emissions on UFPs by conducting a model sensitivity simulation with a lower bound of DMA to NH_3 emissions ratio of 0.003 (reduced by a factor of 5) based on Ge et al.[24] This low DMA emissions case (solid blue line, Figure 1A) reduces simulated UFP number concentrations by a factor of 6 compared to the default simulation (default simulation applies higher DMA emissions, represented by the solid red line in Figure 1A), and underestimates measured particle number concentrations substantially (compared to the observed black line in Figure 1A). In summary, the average DMA to NH_3 emissions ratio can explain the aircraft-observed UFP concentrations in smoke plumes, whereas a lower bound of DMA emissions substantially underestimates observed UFP.

Freshly formed ELVOCs by oxidation of organics in smoke

When DMA emissions in fires are low, explaining UFPs observed by the aircraft in smoke plumes requires a compensating addition of freshly formed ELVOCs that are produced by the oxidation of organic gases emitted by vegetation fires. These freshly formed ELVOCs could grow the smaller amounts of nucleated clusters (compared to when DMA emissions are higher) by compensating for their losses through coagulation and to CSs.[42] Recent laboratory and field measurements indicate the presence of substantial ELVOCs in biomass burning[27,28]; however, the gas-phase yields of ELVOCs from biomass burning await detailed chemical measurements. The ELVOCs govern the survival probability and growth of nucleated clusters to UFPs as determined for biogenic monoterpene oxidation products previously, but ELVOCs from biomass burning are currently not included in models due to the lack of measurements and knowledge of their formation mechanisms in smoke.

To evaluate how ELVOCs from biomass burning could impact UFPs, we performed another model sensitivity test (Figure 1A, "low DMA emission w/biomburn ELVOC") by assuming that the biomass-burning low volatility organic gases corresponding to the lowest volatility bin with C^* of 0.01 $\mu g\ m^{-3}$ within the VBS_{SOM} (VBS-statistical oxidation model) framework (Table S2) are oxidized to ELVOCs (C^* of 10^{-5} $\mu g\ m^{-3}$) instantly within the model chemistry timestep of 5 min.

Our simulation shows that this estimate represents a biomass-burning source of ELVOCs with concentrations <10 pptv over the Amazon (Figure S4E). It has been suggested that multigenerational chemistry of organic gases (with OH radicals) increases the autooxidation and yields of highly oxygenated species[43] due to increasing OH reaction rate coefficients and faster hydrogen-shift reactions of oxidized intermediates compared to the parent hydrocarbons. The lowest volatility species within our biomass-burning VBS framework represents the most oxidized intermediates. Assuming that our lowest volatility species is instantly oxidized to ELVOCs due to accelerating multigenerational chemistry that aids autooxidation likely represents an upper bound on the biomass-burning ELVOC yields as described further in the experimental procedures section upper bound of ELVOCs formed in vegetation fire smoke.

Since the lower bound of DMA emissions substantially underestimates UFP, we combined it with this upper bound ELVOC yield to increase simulated UFPs. Figure 1A shows that this sensitivity case (dashed blue line, "low DMA emission w/biomburn ELVOC") greatly increases UFP concentrations and is in much better agreement with observations and the default simulation (black line, higher DMA emissions without fire ELVOCs). This improved agreement occurs because the reduced DMA emissions in this sensitivity simulation are compensated for by including a source of ELVOCs from the oxidation of biomass-burning organic gases that grow more of the newly nucleated clusters to larger sizes, reducing their coagulation scavenging. Note that with the knowledge of the SD (from, for example, measurements) coagulation rates can be predicted with relatively good accuracy. Consistent with the above definition of fire-affected airmasses averaged over the top 5th percentile BBOA threshold, averaging WRF-Chem results over the top 50th percentile BBOA (Figure S2) shows that the default simulation and the sensitivity case corresponding to the low DMA emission with biomburn ELVOC from fires show the best agreement with measurements. Both the DMA emissions and the ELVOC yields within fire-affected airmasses need to be constrained by future measurements since their combined effect is a substantial increase in UFP number concentrations within fire-affected locations.

Chemical composition of UFPs

The WRF-Chem default simulation indicates that secondary inorganic aerosols, including sulfate, ammonium, and DMA (not shown), dominate the freshly nucleated particle composition at a 1- to 3-nm-diameter size range (Figure S5A). Further growth of these particles is promoted by SOA formation. However, for the sensitivity simulation with lower bound DMA emissions and upper bound ELVOCs from biomass burning, BBSOA formation contributes 30–80% of 1- to 3-nm particle composition (Figure S5C), with their remaining mass fractional composition attributed to inorganic aerosols. Within fire-affected airmasses, OH radical oxidation of phenols, furans, and heterocyclic aromatic compounds causes the formation of BBSOA. Both default and low DMA emission with biomburn-ELVOC simulations indicate that BBSOA contributes ~70%–80% to the composition of particles in the diameter size range of 5–10 nm (Figures S5A and S5C) and the early stages of particle growth. In contrast, over the background Amazon, monoterpene SOA contributes ~90% of the composition of particles in the size range of 5–10 nm (Figure S5E). It is noteworthy that the summed contributions of background monoterpene SOA and SOA formed by oxidation of monoterpenes emitted in biomass-burning smoke (referred to as Terpene SOA in Figure S5) to NPF within fire-influenced regions are already included in all of our model simulations, and WRF-Chem simulations show that within fire smoke, monoterpene ELVOC contributions to 1- to 3-nm-diameter particle composition are negligible (Figures S5A and S5C). Although 5- to 10-nm particles do not contribute substantial amounts to total submicron organic aerosol mass, which is mostly in diameter size bins >100 nm (Figures S5B, S5D, and S5F), these 5- to 10-nm size range particles greatly contribute to UFP number concentrations. Within fresh fire plumes, primary BBOA contributes a greater fraction of submicron organic aerosol mass (~30%) for larger particles (>100 nm diameter), similar to the predicted contribution of BBSOA to these larger particles (Figures S5A and S5C).

Model measurement comparisons on another day (September 25, 2014) consistently show that the DMA + H_2SO_4 nucleation mechanism is the dominant nucleation mechanism within fire-influenced regions. Simulations with average DMA emissions (red solid line, Figures S6A and S6B) and/or lower bound DMA emissions with an upper bound estimate of biomass-burning ELVOCs (blue dashed line, Figures S6A and S6B) are needed to explain UFP number concentrations measured by the FIMS instrument onboard the G-1 aircraft (black solid line, Figure S6). When biomass-burning ELVOCs are not included, the lower bound DMA emissions case (blue solid line, Figures S6A and S6B) underestimates UPF number concentrations compared to measurements (black solid line) by a factor of 2 for both definitions of model-simulated fire-affected airmasses (UFP number averaged over top 5th percentile in Figure S6A and top 50th percentile in Figure S6B).

Model evaluation with HALO aircraft measurements

In addition to the US Department of Energy (DOE) G-1 aircraft, German high altitude and long-range research (HALO) aircraft intersected fresh fire plumes on September 30, 2014. Although the HALO measurements of fire-affected airmasses were outside our modeling domain, they too were the result of vegetation fires like those occurring within our domain. The mean particle number concentrations (>20 nm diameter) measured by the condensation particle counter (CPC) onboard HALO aircraft at 1- to 2-km altitudes within fire-affected regions were ~4,000 cm^{-3} with a standard deviation of 5,000 cm^{-3}, whereas the average background particle number concentrations measured by HALO on a cleaner day (September 28) are ~800 cm^{-3} (lower than fire affected air by a factor of 5). Consistent with these observations, the default model simulation predicts particle concentrations (>20 nm diameter) of 3,000–6,000 cm^{-3} within fire-affected airmasses across the entire domain on September 30, 2014, while simulated background particle number concentrations are lower by a factor of 4–5. Turning nucleation off in a WRF-Chem sensitivity simulation decreases the simulated particle number (>20 nm diameter) within fire-affected airmasses by up to a factor of ~2 and decreases smaller UFPs with diameters <20 nm by up to an order of magnitude compared with the default model. Consequently, nucleation within fire-affected regions greatly increases the UFP number. The impacts of these large enhancements in UFP number concentrations within fire-affected airmasses compared to the background Amazon on clouds and precipitation are investigated using WRF-SBM simulations as discussed in the following section.

Aerosol-cloud interactions simulated by the SBM model

To understand how changes in ultrafine and larger aerosol particles within fire plumes could affect clouds and precipitation, we conducted simulations using the WRF-SBM model at a 0.5-km grid spacing (much finer grid spacing compared with the WRF-Chem grid spacing of 10 km) over a 250 × 250-km domain centered over the Manaus urban region (red rectangle in Figure S1) for the September 30 case that we mainly studied for the fire NPF. This case had scattered deep convective storms, which developed from shallow cumuli and represent a typical weather type in the Amazon (transition of shallow to deep convective clouds). The fire plume interactions with the deep clouds make it a perfect case for a demonstration of the fire aerosol impact. For the September 25 case, the fire plume did not interact with deep convective clouds as much as on September 30; therefore, it is not considered in this part. Aerosol SD, vertical profile, and hygroscopicity including both background and fire aerosols from WRF-Chem are applied in the WRF-SBM simulations, and they affect clouds and precipitation in the WRF-SBM model. Additional details about the WRF-SBM model are provided in the experimental procedures.

In addition to the baseline default fire simulation (Fire), we conducted additional sensitivity simulations, including a background Amazon simulation (Background), a simulation with nucleation turned off throughout the atmospheric column (Fire_noNPF), and a simulation with nucleation turned on only within the planetary boundary layer (PBL) but with nucleation turned off above the PBL (Fire_pblNPF). For each of these simulations, the initial particle SD, the vertical profile of aerosols, and hygroscopicity were obtained from the WRF-Chem simulation averaged over the inner WRF-SBM domain (Figures S7A and S7B). The difference between the simulations of Fire and Background represents the combined effect of the primary particle emissions by wildfires and the nucleation in wildfires, while the difference between the Fire and Fire_noNPF simulations represents the effect of the nucleation within fire-influenced airmasses.

Impacts of particles on clouds and precipitation

Radar reflectivity measurements are helpful for assessing model performance in simulating clouds and precipitation. Higher radar reflectivity generally indicates stronger precipitation. The simulated reflectivity from the Fire simulation agrees well with the radar observations in the intensity and peak time (Figure S8). The observed two large deep convective storms with heavy precipitation (Figure S8, top left) are simulated well in the Fire simulation, except that the locations are shifted northeastward (top right). The observed frequency of reflectivities >55 dBZ (decibel relative to Z) is ~0.28%, and Fire simulates a value of 0.3% (Figure S9). In contrast, the simulated reflectivity is significantly weaker in Background and Fire_noNPF simulations, which lack the large reflectivities (>55 dBZ) found in the Fire simulation. The Fire_pblNPF simulation captures the large reflectivities similar to the Fire simulation, which shows that NPF within the PBL is critical for simulating the large reflectivities. For the rain rate, the radar-retrieved values at 1.5 km above ground are used for the comparison with modeled surface precipitation (Figure 3). It is clear that the observed timing and magnitude of peak rain rate (Figure 3A), as well as the frequency of heavy rain rates (>15 mm h^{-1}; Figure 3B), are much better simulated in Fire (red) and Fire_pblNPF (orange) compared to Background (black) and Fire_noNPF (blue).

By comparing the Fire simulation (red line) with the Background simulation (black line), we show that the fire aerosols (1) increase the accumulated precipitation integrated over the domain from 14:00 UTC on September 30 to 01:00 UTC on October 1 by ~8%, (2) increase the intensity of peak rain rate by ~9% (Figure 3A) and the frequencies of heavy rain rates by ~175% (>15 mm h^{-1}; Figures 3B and 3C), and (3) delay the timing of the initial rain and the peak precipitation by ~40 min (Figure 3A). These are the combined effects of both UFP and larger particles from fires. The NPF within fire-affected

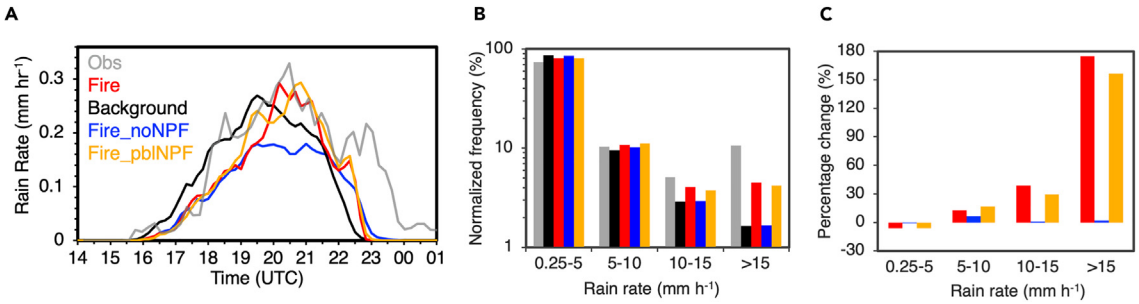

Figure 3. Rain rates observed from radar and predictions by the WRF-SBM model

(A–C) Time series of domain-averaged rain rates (A); normalized frequencies of rain rates for Observations (gray), Background (black), Fire (red), Fire_noNPF (blue), and Fire_pblNPF (orange) from 14:00 UTC September 30–01:00 UTC October 1 (B); and percentage changes in normalized frequencies with respect to Background (C). The observed rain rates are computed from S-band radar reflectivity at 1.5 km above the ground using the equation $Z = 174.8R^{1.56}$, derived from Joss-Waldvogel disdrometer data obtained by the CHUVA campaign near Manacapuru, Brazil during the wet season of early 2014,[44] where R is rain rate (mm h^{-1}) and Z is reflectivity (dBZ). Since the terrain is low in this region, the reflectivity at 1.5 km is reliable and more comparable to the surface rain rates than the retrieved values at the 2.5-km altitude used by Tang et al.[44]

airmasses, which mainly forms UFPs, increases the accumulated precipitation and peak precipitation rate by ~19% and 63%, respectively, and enhances the frequency of heavy rain rates (>15 mm h^{-1}) (difference between blue and red lines in Figure 3B) by ~170%. Thus, the enhancement in precipitation is mainly a result of the UFPs from NPF within the smoke plumes. The smaller magnitudes in the total fire aerosol effects (difference between red and black lines in Figure 3A) compared to the NPF effects (difference between red and blue lines) are because of the offset from the effect of the large particles, which delays and suppresses precipitation, as clearly shown by comparing Fire_noNPF (blue) with Background (black) in Figure 3A. The precipitation properties in Fire_pblNPF (shutting off nucleation in the upper troposphere) are similar to those in the Fire simulation, indicating that NPF within the PBL in fire plumes is mainly responsible for the UFP precipitation effects.

The enhanced precipitation by fire aerosols and the NPF correspond well to the enhanced convective intensity (Figure S10). The increases in the updraft intensity (mean of the top 25th percentile) are large (>50%) between 4 and 7 km and above 11 km by fire aerosols (red vs. black lines in Figure S10), and the increases are mainly due to NPF (red vs. blue lines in Figure S10). The enhanced convective intensity and precipitation are mainly due to larger latent heat from the enhanced condensation because of the activation of a large number of UFPs in the deep convective clouds. In the Fire simulation, cloud droplet number concentrations are increased by up to 1,200% relative to Background (red line, Figure S11B) at ~4- to 6-km altitudes. In the absence of NPF, the Fire_noNPF simulation (blue line) predicts much smaller increases in the cloud droplet number concentration of ~300% compared to Background, mainly due to the activation of larger accumulation-sized particles. Peaks in the cloud droplet number correspond to the elevated levels above cloud bases (>3 km), where vertical velocity and SS are higher. This effect of UFPs through the "water-phase invigoration" or "condensational invigoration" mechanism was shown in an earlier study in this region[18] as well as in the Houston, Texas region.[38] The larger aerosol particles from fires (larger than the sizes of UFPs), which can be activated at cloud base, compete for water vapor forming smaller droplets at the beginning of cloud formation, and these smaller droplets delay (Figure 3A, red vs. black lines) and suppress the rain formation, especially at lower rain rates of 0.25–5 mm h^{-1} (Figure 3C). However, UFPs do not cause a delay in precipitation since they cannot be activated until rain forms.[18]

The simulated case is a typical development of shallow to deep clouds in the Amazon region. Shallow warm clouds with cloud tops below a 4-km altitude start developing into mixed-phase clouds (cloud tops <9 km) at ~16:00 UTC and further grow into deep convective clouds with cloud tops at ~9–14 km after 19:10 UTC (Figure S12A). Aerosols formed in fire-affected airmasses lead to a 77% increase in deep clouds (cloud top heights >9 km and cloud thickness >9 km; Figure 4B) and a 152% increase in their stratiform/anvil clouds (cloud tops >9 km but cloud thickness <5 km; Figure 4B). At the same time, mixed-phase clouds with cloud tops of 5–9 km and cloud thickness of 2–8 km are reduced by ~50% because more of these clouds grow into deep clouds due to the invigoration by the fire aerosols. NPF in the PBL is mainly responsible for the changes in mixed-phase and anvil clouds, but nearly 45% of the increase in the occurrence of deep convective clouds by fires is not contributed by the NPF in the PBL (red vs. orange in Figure 4B). As shown in Figure S11B, the increase in droplet concentrations above 4-km altitudes in Fire_pblNPF (orange) from Background is ~40% less compared with Fire (red). Therefore, the NPF above PBL contributes to the droplet nucleation in the mixed-phase regime (above 4 km) and helps the formation of deep convective clouds, although it does not contribute to precipitation as much (discussed above in Figure 3). There is limited change in shallow cloud fraction. Figures S12B–S12D show the evolution of cloud fraction with time and altitudes, which mix different cloud types. Overall, we see large increases in cloud fraction at the upper levels (deep clouds and their anvils) and decreases in cloud fraction at middle levels (mixed-phase) by fire aerosols and NPF.

Ultrafine particles from NPF within fire-affected airmasses are mainly responsible for the enhanced deep clouds and their anvils, as well as the reduced occurrences of the mixed-phase clouds as shown by the differences between Fire and Fire_noNPF in Figures 4B and S12C. The enhanced updraft intensity (Figure S10) due to the latent heat release from the

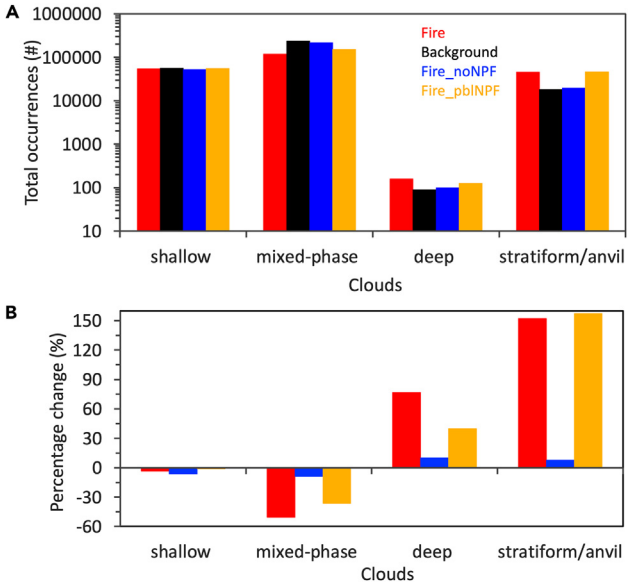

Figure 4. Cloud-type occurrences from WRF-SBM model simulations

(A) Occurrences of thick shallow, mixed-phase, deep clouds, and stratiform and anvil clouds for the simulations Fire (red), Background (black), Fire_noNPF (blue), and Fire_pblNPF (orange) over the time period from 14:00 UTC September 30–01:00 UTC October 1.

(B) Percentage changes in the occurrences of these cloud types relative to the Background. Clouds are identified with the hydrometeor (cloud droplet, ice, and snow particles) mixing ratio $>10^{-5}$ kg kg^{-1}.Thick shallow clouds are defined as clouds with cloud top heights <4 km and cloud thickness >1 km. Mixed-phase clouds are defined as clouds with a cloud top height of 5–9 km and cloud thickness of 2–8 km. Deep clouds are defined as clouds with a cloud top height >9 km and cloud thickness >9 km. Stratiform and anvil clouds are defined as clouds with a cloud top height >9 km and cloud thickness <5 km.

activation of UFPs is the reason for the increased occurrence of deep clouds and the reduced occurrence of mixed-phase clouds. Enhanced convection contributes to the increase in anvil clouds, but the most important reason for the increase in anvil clouds is the reduced ice particle size and fall speed that retard cloud dissipation, as shown in earlier studies.[45] Both UFPs and larger fire aerosols can contribute to reducing ice particle size and fall speeds; consequently, the increased cloud anvils are also seen in the case without UFPs (i.e., Fire_noNPF). Over the entire simulated period (from 14:00 UTC on September 30 to 01:00 UTC on October 1), UFPs slightly increased shallow clouds (Figure 4). The combined fire effect is a slight reduction in shallow clouds, suggesting that the larger aerosol particles reduce shallow clouds. These large aerosol particles are activated around cloud bases and compete for water vapor, forming numerous smaller droplets, which experience enhanced evaporation, resulting in the entrainment mixing of drier air into clouds, possibly contributing to the reduction of shallow clouds.

Note that in the upper troposphere at altitudes >9 km, the nucleation of ultralow volatility organics (ULVOCs, $C^* < 3 \times 10^{-9}$ μg m^{-3}) formed by biogenic VOC oxidation products represented by the R2D-VBS mechanism leads to the formation of a large number of particles throughout the domain (within both background and fire-affected locations, as shown by black and red lines, respectively, in Figure S7B). Our sensitivity test that turns off the nucleation above PBL shows nearly no effect on cloud droplet number concentrations in the upper troposphere (at altitudes >9 km). This is because the UFPs in the upper troposphere (mainly composed of SOA) are not activated to become cloud droplets (Figure S11), probably due to low temperatures and low water vapor concentrations at >9-km altitudes and resultant low SS with respect to liquid water at high altitudes.

DISCUSSION

Vegetation fires in many parts of the globe pose significant risks to air quality, climate, clouds, precipitation, and radiative forcing. The interactions of aerosols with clouds and precipitation constitute one of the largest uncertainties in understanding the climate sensitivity to greenhouse gases. While current models include effects of larger accumulation-mode primary particles directly emitted by fires on clouds, UFP predictions in global climate models might be biased low since these models often do not include nucleation-mode particles, lack detailed treatments of efficient nucleation and growth mechanisms, and lack biomass-burning sources of key nucleating species such as DMA and ELVOCs (as shown in this study) that are needed to form UFPs, especially when CSs of low volatility vapors on fire aerosol surface areas are large. Our WRF-Chem simulations include several nucleation mechanisms and SOA processes based on laboratory measurements and have been validated with field measurements in several places such as the Amazon and over China.[33–35] We use finer grid spacing (~10 km) compared to coarse grid resolution in global models (~100 km) and resolve the entire particle SD ranging from 1 nm to 10 μm with much finer resolutions than global models. Note that the aerosol heterogeneity in vegetation fire plumes finer than the 10-km grid scale is not represented in our WRF-Chem simulations. However, this uncertainty in simulating aerosol heterogeneity should not affect the main conclusions in this study since we focus on statistical averages across an ensemble of local fire plumes that are already diluted when they are entrained into cloud bases.

Analyzing aircraft measurements over the Amazon rainforest, we provide compelling evidence for the observed increase in UFP number concentrations within vegetation fire-affected airmasses. The large increase in CSs in wildfire smoke plumes compared to the background requires an equivalent increase in the production rates of vapors contributing to nucleation and growth. Based on the pseudo-steady-state approximation (PSSA) for nucleating species, which is elaborated on in the experimental procedures section compensating CSs with smoke sources of nucleating species, sufficient steady-state concentrations of nucleating species are needed to explain the aircraft-observed UFP concentrations in smoke. As shown in our previous study, within the Manaus urban plume over the Amazon, the ternary organic + H_2SO_4 nucleation was the key mechanism needed to explain particle number concentrations,[34] but it was not sufficient to explain UFP in biomass-burning plumes in this study.

To explain the observed UFP number in fire-affected airmasses, one of the most efficient nucleation mechanisms, DMA + H_2SO_4 nucleation along with the biomass-burning source

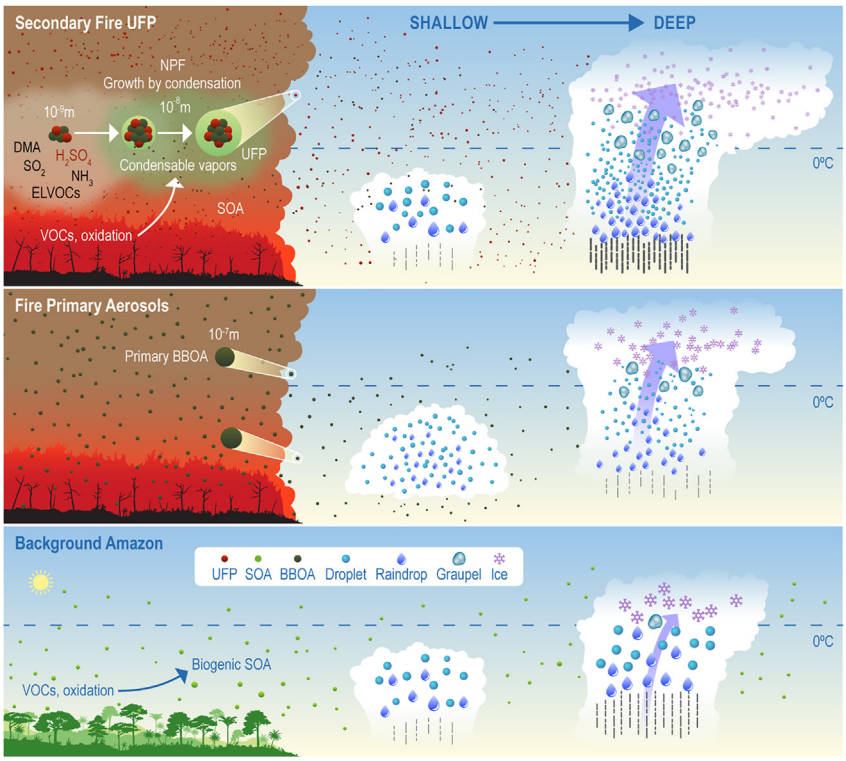

Figure 5. Schematic of UFP formation in biomass-burning smoke and their effects on clouds

Secondary UFPs in biomass-burning smoke (top) might be formed by nucleation, including the DMA + H_2SO_4 mechanism and growth of nucleated clusters through the condensation of oxidized vapors (including ELVOCs) and SOA formation, despite the large losses of condensable low volatility vapors (determined by CS) and the coagulation losses of particles. The effects of UFPs on clouds and precipitation (top) and the effect of primary BBOAs (large particles, center) compared with the background Amazon condition representing a low number of large particles (bottom) are also shown. The dashed line in each panel shows the freezing level. The shallow and deep cloud stages in storm development are depicted from left to right. UFPs cause a stronger storm with a larger anvil and heavier rain after the storm has developed (top right) compared to the primary BBOA from fires (center rightmost panel) and background Amazon (bottom rightmost panel). The primary BBOAs (large particles, center panel) delay and suppress rain compared to background particles (bottom panel). The deep clouds (rightmost panels) are larger with a larger anvil due to much more numerous but smaller ice particle sizes in the top panels compared to the center and bottom panels.

of DMA emissions (elaborated in the experimental procedures section DMA emissions in biomass-burning fires), is needed to compete with the condensation and coagulation sinks in smoke. Without this nucleation, the model underpredicts observed UFP number concentrations by orders of magnitude, as shown in Figure 1A. This is because freshly nucleated particles do not survive coagulation and CSs in biomass-burning plumes unless there is a source of these particles (e.g., nucleation and growth), as described in the supplemental experimental procedures section idealized 0-D box model simulations for assessing the role of coagulation, nucleation, and particle growth. We also show that a lower bound of DMA emissions could explain the observed UFP number if it is aided by the production of gas-phase ELVOCs in biomass-burning smoke (see the experimental procedures section upper bound of ELVOCs formed in vegetation fire smoke), and small ELVOC concentrations ~10 pptv in biomass-burning smoke might be sufficient to grow the nucleated clusters. Measurements of both DMA and gas-phase ELVOCs in biomass-burning smoke are needed to further constrain the processes of NPF. A further support for our conclusions suggesting that UFPs in vegetation fires are mostly secondary is that field measurements over the Amazon show that a negligibly small number fraction (<0.5%) of black carbon cores are in the UFP diameter size range (<50 nm diameter),[46] and pure black carbon particles are not good CCN due to their low hygroscopicity (see the supplemental experimental procedures section role of black carbon).

The contrasting influence of UFPs formed in fires on clouds and precipitation compared to larger accumulation-mode aerosols directly emitted from fires described in this work is schematically illustrated in Figure 5. Fire UFPs may notably increase the frequencies of deep convective clouds and their stratiform and anvil clouds, as well as the heavy precipitation rates (Figure 5, top vs. bottom). The enhancements of deep clouds and precipitation are mainly a result of the invigoration effect by ultrafine aerosols from NPF within fire-affected airmasses through enhanced condensation, whereas the larger particles from fires increase droplets around cloud bases compared to the background Amazon and cause a delay and reduction in precipitation (Figure 5, middle vs. bottom). We find that in our investigated case, the effect of ultrafine aerosols is dominant, which is consistent with a previous investigation that studied the impact of urban emissions of ultrafine aerosols.[18] However, the vegetation fire aerosols investigated here are unique since they contain both ultrafine aerosols and larger CCN-sized aerosols. Note that we use this excellent case that is strongly influenced by fire plumes to demonstrate the potential fire aerosol impacts on the clouds and precipitation. The results from this single (although typical) case may not be generalized to other cases. Also, the role of radiative feedback of biomass-burning aerosols in clouds could be significant in the plume source regions. For the test cases that we simulated in this work, the plume is diluted, and the fire aerosols are entrained into the clouds; therefore, we focused on the impacts of NPF on CCN and clouds and did not consider the radiative effect of fire aerosols in the WRF-SBM model; however, our WRF-Chem simulations included aerosol-cloud-radiation interactions.

As vegetation fires intensify in many parts of the world, biomass-burning UFPs could nonlinearly impact climate sensitivity to greenhouse gases through their effects on

deep clouds and precipitation. While larger primary fire aerosols could delay rain and suppress precipitation, we find that UFPs in fires may enhance deep clouds and precipitation in our investigated case. To better understand the influence of biomass burning on past and future climates, the formation of secondary UFPs from biomass burning and their effects on clouds and precipitation needs to be considered in global models. In addition, these UFPs are expected to exacerbate air quality and human health due to their ability to deposit into the lower respiratory tract. Our study opens new research frontiers by shedding light on the processes related to secondary UFPs in biomass-burning smoke.

EXPERIMENTAL PROCEDURES

Resource availability

Lead contact

Further information and requests for resources and reagents should be directed to and will be fulfilled by the lead contact, Manish Shrivastava (manishkumar.shrivastava@pnnl.gov).

Materials availability

This research did not generate new unique materials.

Data and code availability

All of the data analyzed during the present study are included in this published article and its supplemental information. Aircraft measurements made during the GoAmazon2014/5 field campaign used in this study are publicly available on the Atmospheric Radiation Measurement (ARM) website: http://campaign.arm.gov/goamazon2014/observations/. The detailed community regional model WRF was used for generating model simulations in this study. Model outputs from WRF-Chem and WRF-SBM that were used to generate figures in this study are available from the corresponding author on reasonable request.

Determining fire-affected airmasses from aircraft data

Aircraft-observed airmasses with relatively fresh smoke influence are identified from acetonitrile, a biomass-burning tracer measured by the proton transfer reaction-mass spectrometry (PTR-MS) instrument onboard the DOE G-1 aircraft, exceeding a threshold of 0.4 ppb, since acetonitrile concentrations decrease with long-range transport and dilution.[47] Background airmasses in measurements and models correspond to locations with minimum biomass-burning influence (defined based on acetonitrile <0.2 ppb in observations and BBOA < 0.01 $\mu g\ m^{-3}$ in the model).

Determining fire-affected airmasses in WRF-Chem

For comparison to smoky airmasses identified by the aircraft, fire-affected airmasses simulated by WRF-Chem are identified as those occurring at the same latitude, longitude, and altitudes (within 2 km) as sampled by the G-1 aircraft, but with primary BBOA concentrations exceeding the top 95th percentiles of simulated BBOA. We also analyzed WRF-Chem-simulated particle SDs averaged across the top 50th percentile of simulated BBOA (Figure S2) to explore the sensitivity of our modeled definition of "fire-affected" airmasses. Figures 1A and S2 show that the definitions of fire-affected airmasses with various model sensitivity simulations produce consistent results. Background airmasses in measurements and models correspond to locations with minimum biomass-burning influence (defined based on acetonitrile <0.2 ppb in observations and BBOA <0.01 $\mu g\ m^{-3}$ in the model).

WRF-Chem 4.2 model configuration

We used the regional WRF-Chem 4.2 model[48,49] at 10-km grid spacings, covering 1,500 × 1,000 km around the Manaus urban area in the Amazon during the dry season covering September 20–October 1, 2014. The National Centers for Environmental Prediction Climate Forecast System version 2 reanalysis data[50] provided the meteorological initial and boundary conditions. Meteorological conditions were spun up for 24 h, followed by 36 h of simulation, while the chemical trace gas and aerosol species from the previous simulation were used as initial conditions (i.e., the chemistry was continuous over the 10-day simulation). The quasi-global WRF-Chem simulation for 2014 provided chemical boundary and initial conditions for trace gases and aerosols.[51] Each particle-phase chemical constituent was represented by 20 size sections ranging from 1 nm to 10 μm as both interstitial and cloud-borne aerosols and both mass and number are tracked in each size section. Inorganic aerosol chemistry in WRF-Chem is represented by the Model for Simulating Aerosol Interactions and Chemistry.[52] In this work, we treat the condensation/evaporation of SOA using the kinetic gas-particle partitioning approach wherein the model calculates the condensation/evaporation of organic gases to homogeneously mixed SOA particles in each size bin using a semi-implicit Eulerian approach with adaptive time stepping based on Zaveri et al.[53] The dynamic gas-particle partitioning approach represents a significant improvement over the previous instantaneous equilibrium partitioning approaches used in WRF-Chem. In addition, limitations to gas-particle mass transfer due to organic particle phase diffusion limitations are explicitly accounted for by calculations of OA viscosity at each grid cell, time step, and aerosol size bin.[54] Biogenic volatile organic compound emissions are derived from the latest version of the Model of Emissions of Gases and Aerosols from Nature (version 2.1), recently coupled within the community land model CLM version 4.0 in WRF-Chem.[55] SOA formed due to the oxidation of monoterpenes is represented using the R2D-VBS framework,[33,34] while that formed from other biogenic and anthropogenic organic gases is represented using the one-dimensional VBS approach.[56] SOA yields vary with oxidant type (OH, O_3, NO_3 radicals) and high/low NO_x conditions, which agreed with field measurements over the Amazon.[33,34,56] However, anthropogenic SOA formation is negligible for the analyses presented in the present paper, since here we focus on background and biomass-burning fire-affected locations. The formation of BBSOA is simulated using a new approach based on the VBS_{SOM}, as described in the three sections within the supplemental experimental procedures: Biomass Burning-SOA Formulation Based on the SOM-TOMAS Model, SOA Formation due to Biomass Burning, and VBS_{SOM} Model and Parameters.

Primary biomass-burning emissions

We included primary biomass-burning emissions, including both gases and aerosols, from the 2014 Quick Fire Emissions Database (QFED) emissions version 2.5 (https://portal.nccs.nasa.gov/datashare/iesa/aerosol/emissions/QFED/v2.5r1/0.1/QFED/). QFED includes particulate emissions, including POA, black carbon, $PM_{2.5}$, and trace gas emissions that include CO, NH_3, NO, and SO_2. POA emitted from biomass burning (same as BBOA) is assumed to be of low volatility, with a C^* of 0.01 $\mu g\ m^{-3}$, causing most of the BBOA to partition to the particle phase. We assumed that BBOA consists of highly viscous species that do not mix with SOA; therefore, BBOA does not affect gas-particle partitioning of SOA and vice versa.[57,58] Within biomass-burning plumes, SOA is formed by the oxidation of semivolatile and volatile organics. Recent field studies show that the ratio of total OA to CO remains almost constant downwind of biomass-burning plumes, likely because the evaporation of the semivolatile fraction of BBOA with dilution is compensated for by an equivalent amount of SOA formation.[59] Thus, the assumed low-volatility BBOA represents net OA formation due to evaporation of the semivolatile BBOA fraction and equivalent BBSOA formation. However, condensation of evaporated BBOA vapors could assist in NPF depending on their volatility and merits exploration in future studies. Formation of BBSOA from volatile organics emitted in biomass-burning plumes is treated separately, as discussed in the following section. The simulated BBSOA dominates the composition of UFP but is comparable to primary BBOA in accumulation-size-range particles (>100 nm). We coupled the gases and aerosols simulated by QFED with the Freitas plume rise parameterization[60] in WRF-Chem. The fire heat fluxes are considered in the Freitas plume rise model in our WRF-Chem simulations following our previous study,[61] which feeds back to the meteorological conditions affecting clouds and aerosols in the simulations (described further in the supplemental experimental procedures section Simulation of Fire Heat Flux, Size, And Plume Injection Height). Almost all fire inventories, including QFED, use a fixed emissions ratio for a given fuel type that is averaged across combustion conditions. For our simulations over the Amazon, we assumed 45% flaming and 55% smoldering for plume rise and heat flux calculations based on the value reported for tropical forests in Table 1 of Freitas et al.[60]

Emissions of BBSOA VOC precursors

We simulate BBSOA by accounting for the oxidation of VOC surrogates from two key precursor classes emitted by wildfires. These VOC precursor classes include (1) oxygenated aromatics (e.g., phenols), (2) a grouping of heterocyclics (e.g., furans), aromatic hydrocarbons (e.g., toluene), biogenic VOCs (e.g., monoterpenes), and alkanes.[62] The molar emissions ratios for these 2 classes are averaged from Fire Influence on Regional and Global Environments Experiment laboratory measurements that sampled a range of fuels such as pine, spruce, and grass shrub, and burning conditions covered smoldering to flaming with a modified combustion efficiency that varied between 0.78 and 0.96 across the experiments. Thus, these experiments cover a range of fuel types and burn conditions (flaming and smoldering), and the derived average emissions ratios are expected to apply widely. Average molar emissions ratios for the oxygenated aromatics and heterocyclics classes with respect to CO were estimated as 9.5 and 25.9 ppb/ppm-CO, respectively, based on chamber experiments performed and reported by Akherati et al.[62] These laboratory emissions ratios also compare well with field measurements based on aircraft and mobile monitoring.[63,64] These ratios are then multiplied with QFED CO emissions to generate their emissions over the Amazon.

Simulating BBSOA from VOC oxidation

The current model simulates BBSOA by accounting for the oxidation of VOC surrogates from the oxygenated aromatic and heterocyclic precursor classes emitted by vegetation fires, as described above. We represent BBSOA formation from these precursors using a VBS_{SOM} approach, with C^* spanning 0.01 to 10^4 $\mu g\ m^{-3}$ (Table S2) based on Akherati et al.,[62] as documented in the supplemental experimental procedures section VBS_{SOM} Model and Parameters. The SOM model integrated with a two-moment aerosol section scheme (SOM-TOMAS) has previously been successfully used to simulate particle number concentrations, including nucleation and growth measured in a flow tube during SOA formation.[42]

Primary BBOA and SOA are assumed to form two separate phases for gas-particle partitioning calculations based on previous measurements showing that SOA and hydrophobic primary OA might not mix in the bulk phase.[57,58] We include primary biomass-burning emissions, with both gases and aerosols, from the 2014 QFED[65] emissions version 2.5.

Compensating CSs with smoke sources of nucleating species

CSs are the first-order loss rates through condensation of low-volatility vapors and are governed primarily by the preexisting particle number SD.[21–23] The concentrations of low volatility vapors (sulfuric acid and ELVOCs) can be assumed to be at a pseudo steady state with their sources and sinks—in other words, the production rate of low-volatility vapors is assumed to equal their loss by condensation to existing particles (CS), which is known as the PSSA.[66]

Thus, the PSSA concentration of gas-phase H_2SO_4 [H_2SO_4] and ELVOCs [ELVOC] can be calculated as $[H_2SO_4] = P_{H2SO4}/CS$, and $[ELVOC] = P_{ELVOC}/CS$, wherein P_{H2SO4} and P_{ELVOC} denote the production rates of H_2SO_4 and ELVOCs in smoke plumes. Nucleation rates are proportional to the product of concentrations of low volatility vapors—for example, the nucleation rate between [H_2SO_4] and biogenic ELVOC (BioOxOrg) is parameterized as[67] $J = k_m[H_2SO_4]^2[BioOxOrg]$, which implies that the nucleation rate is proportional to $1/CS^3$ when production rates of H_2SO_4 and BioOxOrg are constant. This reasoning implies that to obtain nontrivial nucleation rates (that are proportional to the product of pseudo-steady-state concentrations of the nucleating species), the production rates of low volatility vapors need to increase with the increase in CSs in smoke plumes.

Biogenic monoterpene ELVOCs

In this work, the concentrations of biogenic monoterpene ELVOCs participating in nucleation are predicted online in WRF-Chem at each model grid and time step. The WRF-Chem/R2D-VBS model used in this study was developed in our previous studies[33,34,68] by incorporating in WRF-Chem version 4.2 the R2D-VBS and its parameterizations as well as an advanced NPF module involving seven NPF pathways. The R2D-VBS systematically simulates the temperature-dependent oxidation chemistry of monoterpenes, including the formation of ULVOCs and ELVOCs that drive organic mediated NPF mechanisms.[30] For implementation into a detailed regional model such as WRF-Chem, where computational costs greatly increase with a simulated number of advected tracers, the R2D-VBS was mapped onto an equivalent one-dimensional VBS (1D-VBS). However, only species with O:C > 0.4 were included in this 1D-VBS, and the total organic concentrations in the ULVOC and ELVOC ranges of the condensed 1D-VBS were used to drive organic-mediated nucleation. The remaining less-oxygenated compounds (with O:C $\leq$ 0.4) do not contribute to nucleation in the model formulation. The 7 different NPF pathways that are implemented in WRF-Chem are binary-neutral and ion-induced NPF (involving H_2SO_4 and H_2O), ternary-neutral and ion-induced NPF (involving H_2SO_4, NH_3, and H_2O), pure organic neutral and ion-induced NPF, and ternary NPF involving organics, H_2SO_4, and H_2O.[33,34] However, we found that these mechanisms greatly underpredict the observed UFP SDs within fire-affected airmasses measured by the FIMS mounted onboard the G-1 aircraft. Therefore, we incorporated our best knowledge of another efficient nucleation mechanism—the DMA + H_2SO_4, previously implemented in WRF-Chem and evaluated with measurements in urban China.[35] Although this DMA + H_2SO_4 mechanism has not been previously implemented and evaluated in biomass-burning smoke, we found that this mechanism closes the large gap between modeled and observed UFP number concentrations observed in fire plumes.

DMA emissions in biomass-burning fires

Biomass burning is one of the main natural sources of DMA emissions.[25] However, the role of DMA emitted by biomass burning on NPF has not been modeled. We included the biomass-burning emissions source of DMA within WRF-Chem. DMA emissions in biomass-burning fires are estimated based on their reported ratios to NH_3 within wildfire plumes based on Ge et al.[24] As described in the main text, we conducted sensitivity simulations with a median and lower bound DMA to NH_3 emissions ratio (0.017 and 0.003, respectively) within fires. Since the lower bound DMA emissions greatly underpredicted the observed UFPs in fires, we conducted a model sensitivity test combining these lower DMA emissions with an upper bound of ELVOCs (ELVOCs defined as species with $C^* \leq 10^{-5}$ $\mu g\ m^{-3}$) within fires. The Manaus urban area is an additional source of DMA emissions, but it affects a much smaller region compared to vegetation fires. The simulated contribution of Manaus DMA emissions to UFP was much lower by a factor of 7 compared to the corresponding vegetation fire source of DMA within the fire-affected airmasses analyzed in this work. To assess how DMA emissions impact our simulated particle number concentrations, we performed a sensitivity test with a lower bound of DMA molar emissions ratio (factor of 5 lower than the default model), as described in the main text. Since the lower bound DMA emissions greatly underpredicted observed UFPs in fires, we conducted a model sensitivity test combining these lower DMA emissions with an upper bound of ELVOCs produced by the oxidation of organic gases emitted by vegetation fires.

Upper bound of ELVOCs formed in vegetation fire smoke

In this study, we assumed that biomass-burning ELVOCs do not participate in nucleation but can still grow the nucleated clusters to larger sizes due to their low volatility, thus increasing the UFP number. Gas-phase ELVOCs in biomass-burning smoke are likely formed by autoxidation and multigenerational oxidation of organic gases emitted in smoke and could greatly enhance the growth of molecular clusters to UFP sizes due to their low volatility. However, due to the complexity of smoke chemistry, the detailed kinetics and reaction mechanisms of ELVOC formation in biomass-burning smoke are unknown. However, using measurements of particle SD evolution in smoke plumes, reasonable upper bounds of ELVOC formation needed to grow molecular clusters in smoke could be estimated. We estimated an upper bound to ELVOC by moving the gas-phase organics within our lowest volatility bin of BBSOA to ELVOC instantaneously. The lowest volatility bin represents the most oxidized and functionalized species in our VBS_{SOM} mechanism, and it has been suggested that the probability of H-shift reaction and autoxidation increases for highly functionalized species. However, large uncertainties persist in the quantification of highly oxygenated organic molecule formation from OH-initiated oxidation sequences involving alkoxy radicals and carbon-centered radicals, especially for aromatic and saturated hydrocarbons. At atmospheric conditions,[43] our assumption represents an upper bound estimate of gas-phase ELVOCs from biomass burning. Particle-phase measurements of biomass-burning-influenced airmasses in both laboratory and field studies indicate the presence of substantial low volatility organics (including ELVOCs)

that could contribute up to 50% of BBOA mass.[27,28] Future measurements at atmospheric-relevant conditions are needed to constrain gas-phase ELVOC yields from biomass-burning smoke to understand NPF.

Cloud and precipitation simulations

To investigate the impacts of biomass-burning aerosols and NPF in fire-affected regions on clouds and precipitation over the Amazon, we conducted deep convection-resolving simulations at 0.5-km grid spacings for a locally occurring convective case on September 30, 2014, using the WRF-SBM model.[38,39] The major advantages of the SBM scheme include (1) allowing aerosols to impact the shape of droplet SD, which is very important for the follow-on microphysics processes such as rain formation and growth processes; (2) calculating SS based on explicit calculation of droplet condensation and evaporation, and so forth. The bulk schemes available in WRF use saturation adjustments for condensation and evaporation, which cannot account for aerosol effects on condensation that are especially important for UFPs.[18,69–71]

The convective case was a typical shallow-to-deep transition case influenced by biomass burning in the Amazon. The low-level wind was northeasterly. The cloud bases were warm (~17°C), with weak wind shear in the lower troposphere. We used the European Center for Medium-Range Weather Forecasts reanalysis version 5 at 0.25° horizontal resolution and 6-h temporal intervals for initial and lateral boundary conditions. The model domain is ~250 × 250 km with 65 vertical levels up to 50 hPa. The modeled dynamic timestep was 3 s, and simulations were initiated at 06:00 UTC on September 29 and run for 24 h. The simulation output frequency used for the analysis was 10 min. The soil moisture was from an operational product from the Center for Weather Forecasting and Climate Research/National Institute of Space Research in Brazil, which is a daily product at 0.25°.[72] The surface albedo, vegetation, and green fraction are documented in Beck et al.[73] Other physics parameterizations used include the Mellor-Yamada-Janjić PBL scheme, the unified Noah land surface scheme, and the rapid radiative transfer model for general circulation model longwave and shortwave radiation.

Description of WRF-SBM simulations

To simulate how different particle SDs and hygroscopicity within ultrafine and accumulation-mode aerosols affect cloud microphysics and precipitation, the default WRF-Chem simulations were used to provide the aerosol SD and vertical distribution (VD) data (Figure S7), as well as hygroscopicity, to the WRF-SBM model simulations. These SDs and VDs were prescribed as initial and boundary conditions to WRF-SBM runs for each simulated timestep of 3 s. The baseline simulation (referred to as "Fire") used the aerosol SDs and VDs from the "Fire-affected airmasses" in the WRF-Chem simulation. We defined the "Fire" hotspots for each atmospheric vertical column where the primary BBOA concentration at cloud base (1- to 2-km altitudes) exceeds the median domain BBOA value of 3 $\mu g\ m^{-3}$ during the entire simulation period. The "Background" run used the aerosol SDs and VDs from the WRF-Chem simulation, excluding fire influence—in other words, where BBOA concentrations were <0.01 $\mu g/m^3$ (background aerosol conditions). Fires produce orders of magnitude higher UFPs and several times higher accumulation-mode aerosol number compared to the background aerosols (Figure 1). To examine the effect from NPF with the vegetation fires in the Amazon, an additional sensitivity test "Fire_noNPF" was conducted, which used the aerosol SDs and VDs from another WRF-Chem simulation with fire emissions turned on but nucleation turned off. To further investigate the relative importance of NPF at low levels (i.e., in the PBL) and high levels (i.e., above PBL), we conducted a sensitivity test "Fire_pblNPF," which takes the aerosol SDs and VDs from the "Fire" simulation for the altitudes within the PBL (<2 km) and those from "Fire_noNPF" for the altitudes above the PBL.

Evaluation of WRF-SBM with radar reflectivity measurements

Radar reflectivity measurements are helpful for assessing model performance in simulating clouds and precipitation. Higher radar reflectivity indicates stronger deep convection and precipitation. We evaluated the simulated composite reflectivity by WRF-SBM with the S-band radar located at Manaus (Figure S8). The observed radar reflectivity reached its largest value of >55 dBZ at 20:36 UTC. The baseline simulation (Fire) agrees well with the observation in the intensity and peak time, although it is slightly shifted in its location. The observed large radar reflectivities are well captured by the Fire simulation, but significantly weaker in the Background and Fire_noNPF simulations. The simulated peak time in the simulations that include the Fire emissions (20:20 UTC in Wildfire, 20:10 UTC in Fire_noNPF, and 20:40 UTC in Fire_pblNPF) is much closer to the S-band radar observations (20:36 UTC) compared to the simulation without fires (19:40 UTC in Background). It is noted that there is a similar frequency of reflectivity >55 dBZ as shown in observations in Fire and Fire_pblNPF, but these larger reflectivities are completely absent in the Background and Fire_noNPF simulations (Figure S9). Our analyses suggest that it is important to consider the Fires and NPF in the model for better simulating deep convective clouds in terms of intensity and timing.

Previous model simulations often do not resolve the nucleation mode of the aerosol size distribution and lack a coupling of advanced SOA and chemistry modules with a sectional cloud microphysics scheme for the explicit treatment of aerosol-cloud interactions. Here, coupling the WRF-Chem and WRF-SBM models with all of these advanced features, we find the critical role of NPF within fire-affected airmasses in forming abundant UFPs, which is manifested in their pronounced influence on clouds and precipitation.

SUPPLEMENTAL INFORMATION

Supplemental information can be found online at https://doi.org/10.1016/j.oneear.2024.05.015.

ACKNOWLEDGMENTS

This research was supported by the US DOE Office of Science, Office of Biological and Environmental Research (BER) through the Early Career Research Program and the DOE BER's Atmospheric System Research program. Funding for data collection onboard the G-1 aircraft and at the ground sites was provided by the ARM Climate Research Facility, a DOE user facility sponsored by the BER. HALO-related work was supported by the Max Planck Society, the DFG (Deutsche Forschungsgemeinschaft, German Research Foundation) Priority Program SPP 1294, the German Aerospace Center (DLR), the BMBF program ROMIC (01LG1205E), Max Planck Society Brazilian foundations FAPESP (São Paulo Research Foundation) grants 2009/15235-8 and 2013/05014-0, FAPEAM, and a wide range of other institutional partners. The Pacific Northwest National Laboratory (PNNL) is operated for the DOE by Battelle Memorial Institute under contract DE-AC06-76RL01830. The Argonne National Laboratory is operated for the DOE by UChicago Argonne, LLC, under contract DE-AC02-06CH11357. J.R.P., S.H.J., and A.A. acknowledge funding from the National Science Foundation (NSF; AGS-1950327), the DOE BER's Atmospheric System Research program (DE-SC0021208), the National Oceanic and Atmospheric Administration (NA17OAR4310001 and NA17OAR4310003), and the US Environmental Protection Agency (R840008). This publication has not been formally reviewed by the US EPA. The views expressed in this document are solely those of the authors and do not necessarily reflect those of the Agency. The US EPA does not endorse any products or commercial services mentioned in this publication. N.M.D. acknowledges funding from the NSF (AGS-2132089). Computational resources for the simulations were provided by the Environmental Molecular Sciences Laboratory (EMSL, a DOE Office of Science user facility sponsored by the BER located at PNNL) and the National Energy Research Scientific Computing Center, which is a US DOE Office of Science user facility operated under contract no. DE-AC02-05CH11231. We thank John Shilling for G-1 PTR-MS measurements of acetonitrile and related discussions and Jian Wang for FIMS measurements onboard the DOE G-1 aircraft.

AUTHOR CONTRIBUTIONS

M.S. conceptualized the study and conducted WRF-Chem simulations. M.S. and J.F. designed the research and wrote the original manuscript. Y.Z. and J.F. conducted WRF-SBM simulations and analyzed the results. B.Z. and J.S. contributed to the NPF modules. M.S. and J.R.P. investigated NPF in smoke using WRF-Chem and a 0-D box model. S.H.J. and A.A. contributed to the BBSOA modules. M.S., J.F., Y.Z., Q.Z.R., and J.Z. generated the visualizations. All of the coauthors contributed to the writing of the paper.

DECLARATION OF INTERESTS

The authors declare no competing interests.

Received: February 1, 2024
Revised: May 27, 2024
Accepted: May 28, 2024
Published: June 21, 2024

REFERENCES

1. Seinfeld, J.H., Bretherton, C., Carslaw, K.S., Coe, H., DeMott, P.J., Dunlea, E.J., Feingold, G., Ghan, S., Guenther, A.B., Kahn, R., et al. (2016). Improving our fundamental understanding of the role of aerosol-cloud interactions in the climate system. Proc. Natl. Acad. Sci. USA *113*, 5781–5790. https://doi.org/10.1073/pnas.1514043113.
2. Shrivastava, M., Cappa, C.D., Fan, J., Goldstein, A.H., Guenther, A.B., Jimenez, J.L., Kuang, C., Laskin, A., Martin, S.T., Ng, N.L., et al. (2017). Recent advances in understanding secondary organic aerosol: Implications for global climate forcing. Rev. Geophys. *55*, 509–559. https://doi.org/10.1002/2016rg000540.
3. Bond, T.C., Streets, D.G., Yarber, K.F., Nelson, S.M., Woo, J.H., and Klimont, Z. (2004). A technology-based global inventory of black and organic carbon emissions from combustion. J. Geophys. Res. *109*, D14203. https://doi.org/10.1029/2003jd003697.
4. Zhang, Y., Fan, J., Shrivastava, M., Homeyer, C.R., Wang, Y., and Seinfeld, J.H. (2022). Notable impact of wildfires in the western United States on weather hazards in the central United States. Proc. Natl. Acad. Sci. USA *119*, e2207329119. https://doi.org/10.1073/pnas.2207329119.
5. Liu, L., Cheng, Y., Wang, S., Wei, C., Pöhlker, M.L., Pöhlker, C., Artaxo, P., Shrivastava, M., Andreae, M.O., Pöschl, U., and Su, H. (2020). Impact of biomass burning aerosols on radiation, clouds, and precipitation over the Amazon: relative importance of aerosol–cloud and aerosol–radiation interactions. Atmos. Chem. Phys. *20*, 13283–13301. https://doi.org/10.5194/acp-20-13283-2020.
6. de Oliveira Alves, N., Brito, J., Caumo, S., Arana, A., de Souza Hacon, S., Artaxo, P., Hillamo, R., Teinilä, K., Batistuzzo de Medeiros, S.R., and de Castro Vasconcellos, P. (2015). Biomass burning in the Amazon region: Aerosol source apportionment and associated health risk assessment. Atmos. Environ. *120*, 277–285.
7. Reddington, C.L., Morgan, W.T., Darbyshire, E., Brito, J., Coe, H., Artaxo, P., Scott, C.E., Marsham, J., and Spracklen, D.V. (2019). Biomass burning aerosol over the Amazon: analysis of aircraft, surface and satellite observations using a global aerosol model. Atmos. Chem. Phys. *19*, 9125–9152. https://doi.org/10.5194/acp-19-9125-2019.
8. Brando, P.M., Soares-Filho, B., Rodrigues, L., Assunção, A., Morton, D., Tuchschneider, D., Fernandes, E.C.M., Macedo, M.N., Oliveira, U., and Coe, M.T. (2020). The gathering firestorm in southern Amazonia. Sci. Adv. *6*, eaay1632.
9. Liu, J.C., Mickley, L.J., Sulprizio, M.P., Dominici, F., Yue, X., Ebisu, K., Anderson, G.B., Khan, R.F.A., Bravo, M.A., and Bell, M.L. (2016). Particulate air pollution from wildfires in the Western US under climate change. Clim. Change *138*, 655–666.
10. Kulmala, M., Vehkamäki, H., Petäjä, T., Dal Maso, M., Lauri, A., Kerminen, V.M., Birmili, W., and McMurry, P.H. (2004). Formation and growth rates of ultrafine atmospheric particles: a review of observations. J. Aerosol Sci. *35*, 143–176. https://doi.org/10.1016/j.jaerosci.2003.10.003.
11. Hennigan, C.J., Westervelt, D.M., Riipinen, I., Engelhart, G.J., Lee, T., Collett, J.L., Pandis, S.N., Adams, P.J., and Robinson, A.L. (2012). New particle formation and growth in biomass burning plumes: An important source of cloud condensation nuclei. Geophys. Res. Lett. *39*, L09805. https://doi.org/10.1029/2012GL050930.
12. Hobbs, P.V., Sinha, P., Yokelson, R.J., Christian, T.J., Blake, D.R., Gao, S., Kirchstetter, T.W., Novakov, T., and Pilewskie, P. (2003). Evolution of gases and particles from a savanna fire in South Africa. J. Geophys. Res. *108*, 8485. https://doi.org/10.1029/2002JD002352.
13. Vakkari, V., Kerminen, V.-M., Beukes, J.P., Tiitta, P., Zyl, P.G., Josipovic, M., Venter, A.D., Jaars, K., Worsnop, D.R., Kulmala, M., and Laakso, L. (2014). Rapid changes in biomass burning aerosols by atmospheric oxidation. Geophys. Res. Lett. *41*, 2644–2651. https://doi.org/10.1002/2014GL059396.
14. Laing, J.R., Jaffe, D.A., and Hee, J.R. (2016). Physical and optical properties of aged biomass burning aerosol from wildfires in Siberia and the Western USA at the Mt. Bachelor Observatory. Atmos. Chem. Phys. *16*, 15185–15197. https://doi.org/10.5194/acp-16-15185-2016.
15. Sakamoto, K.M., Allan, J.D., Coe, H., Taylor, J.W., Duck, T.J., and Pierce, J.R. (2015). Aged boreal biomass-burning aerosol size distributions from BORTAS 2011. Atmos. Chem. Phys. *15*, 1633–1646. https://doi.org/10.5194/acp-15-1633-2015.
16. Hodshire, A.L., Ramnarine, E., Akherati, A., Alvarado, M.L., Farmer, D.K., Jathar, S.H., Kreidenweis, S.M., Lonsdale, C.R., Onasch, T.B., Springston, S.R., et al. (2021). Dilution impacts on smoke aging: evidence in Biomass Burning Observation Project (BBOP) data. Atmos. Chem. Phys. *21*, 6839–6855. https://doi.org/10.5194/acp-21-6839-2021.
17. Davidson, E.A., de Araújo, A.C., Artaxo, P., Balch, J.K., Brown, I.F., C. Bustamante, M.M., Coe, M.T., DeFries, R.S., Keller, M., Longo, M., et al. (2012). The Amazon basin in transition. Nature *481*, 321–328. https://doi.org/10.1038/nature10717.
18. Fan, J., Rosenfeld, D., Zhang, Y., Giangrande, S.E., Li, Z., Machado, L.A.T., Martin, S.T., Yang, Y., Wang, J., Artaxo, P., et al. (2018). Substantial convection and precipitation enhancements by ultrafine aerosol particles. Science *359*, 411–418. https://doi.org/10.1126/science.aan8461.
19. Svensmark, H., Enghoff, M.B., Svensmark, J., Thaler, I., and Shaviv, N.J. (2024). Supersaturation and Critical Size of Cloud Condensation Nuclei in Marine Stratus Clouds. Geophys. Res. Lett. *51*, e2024GL108140. https://doi.org/10.1029/2024GL108140.
20. Pöhlker, M.L., Ditas, F., Saturno, J., Klimach, T., Hrabě de Angelis, I., Araùjo, A.C., Brito, J., Carbone, S., Cheng, Y., Chi, X., et al. (2018). Long-term observations of cloud condensation nuclei over the Amazon rain forest – Part 2: Variability and characteristics of biomass burning, long-range transport, and pristine rain forest aerosols. Atmos. Chem. Phys. *18*, 10289–10331. https://doi.org/10.5194/acp-18-10289-2018.
21. Casquero-Vera, J.A., Pérez-Ramírez, D., Lyamani, H., Rejano, F., Casans, A., Titos, G., Olmo, F.J., Dada, L., Hakala, S., Hussein, T., et al. (2023). Impact of desert dust on new particle formation events and the cloud condensation nuclei budget in dust-influenced areas. Atmos. Chem. Phys. *23*, 15795–15814. https://doi.org/10.5194/acp-23-15795-2023.
22. Du, W., Cai, J., Zheng, F., Yan, C., Zhou, Y., Guo, Y., Chu, B., Yao, L., Heikkinen, L.M., Fan, X., et al. (2022). Influence of Aerosol Chemical Composition on Condensation Sink Efficiency and New Particle Formation in Beijing. Environ. Sci. Technol. Lett. *9*, 375–382. https://doi.org/10.1021/acs.estlett.2c00159.
23. Tuovinen, S., Kontkanen, J., Jiang, J., and Kulmala, M. (2020). Investigating the effectiveness of condensation sink based on heterogeneous nucleation theory. J. Aerosol Sci. *149*, 105613. https://doi.org/10.1016/j.jaerosci.2020.105613.
24. Ge, X., Wexler, A.S., and Clegg, S.L. (2011). Atmospheric amines – Part I. A review. Atmos. Environ. *45*, 524–546. https://doi.org/10.1016/j.atmosenv.2010.10.012.
25. Yang, Y., Zhao, T., Jiao, H., Wu, L., Xiao, C., and Guo, X. (2022). Types and Distribution of Organic Amines in Organic Nitrogen Deposition in Strategic Water Sources. Int. J. Environ. Res. Publ. Health *19*, 4151.
26. Yokelson, R.J., Burling, I.R., Gilman, J.B., Warneke, C., Stockwell, C.E., de Gouw, J., Akagi, S.K., Urbanski, S.P., Veres, P., Roberts, J.M., et al. (2013). Coupling field and laboratory measurements to estimate the emission factors of identified and unidentified trace gases for prescribed fires. Atmos. Chem. Phys. *13*, 89–116. https://doi.org/10.5194/acp-13-89-2013.

27. Shetty, N., Liu, P., Liang, Y., Sumlin, B., Daube, C., Herndon, S., Goldstein, A.H., and Chakrabarty, R.K. (2023). Brown carbon absorptivity in fresh wildfire smoke: associations with volatility and chemical compound groups. Environ. Sci. Atmos. *3*, 1262–1271. https://doi.org/10.1039/D3EA00067B.

28. Brege, M.A., China, S., Schum, S., Zelenyuk, A., and Mazzoleni, L.R. (2021). Extreme Molecular Complexity Resulting in a Continuum of Carbonaceous Species in Biomass Burning Tar Balls from Wildfire Smoke. ACS Earth Space Chem. *5*, 2729–2739. https://doi.org/10.1021/acsearthspacechem.1c00141.

29. Bianchi, F., Kurtén, T., Riva, M., Mohr, C., Rissanen, M.P., Roldin, P., Berndt, T., Crounse, J.D., Wennberg, P.O., Mentel, T.F., et al. (2019). Highly Oxygenated Organic Molecules (HOM) from Gas-Phase Autoxidation Involving Peroxy Radicals: A Key Contributor to Atmospheric Aerosol. Chem. Rev. *119*, 3472–3509. https://doi.org/10.1021/acs.chemrev.8b00395.

30. Schervish, M., and Donahue, N.M. (2020). Peroxy radical chemistry and the volatility basis set. Atmos. Chem. Phys. *20*, 1183–1199. https://doi.org/10.5194/acp-20-1183-2020.

31. Hallquist, M., Wenger, J.C., Baltensperger, U., Rudich, Y., Simpson, D., Claeys, M., Dommen, J., Donahue, N.M., George, C., Goldstein, A.H., et al. (2009). The formation, properties and impact of secondary organic aerosol: current and emerging issues. Atmos. Chem. Phys. *9*, 5155–5236. https://doi.org/10.5194/acp-9-5155-2009.

32. Riipinen, I., Pierce, J.R., Yli-Juuti, T., Nieminen, T., Häkkinen, S., Ehn, M., Junninen, H., Lehtipalo, K., Petäjä, T., Slowik, J., et al. (2011). Organic condensation: a vital link connecting aerosol formation to cloud condensation nuclei (CCN) concentrations. Atmos. Chem. Phys. *11*, 3865–3878. https://doi.org/10.5194/acp-11-3865-2011.

33. Zhao, B., Shrivastava, M., Donahue, N.M., Gordon, H., Schervish, M., Shilling, J.E., Zaveri, R.A., Wang, J., Andreae, M.O., Zhao, C., et al. (2020). High concentration of ultrafine particles in the Amazon free troposphere produced by organic new particle formation. Proc. Natl. Acad. Sci. USA *117*, 25344–25351. https://doi.org/10.1073/pnas.2006716117.

34. Zhao, B., Fast, J.D., Donahue, N.M., Shrivastava, M., Schervish, M., Shilling, J.E., Gordon, H., Wang, J., Gao, Y., Zaveri, R.A., et al. (2021). Impact of Urban Pollution on Organic-Mediated New-Particle Formation and Particle Number Concentration in the Amazon Rainforest. Environ. Sci. Technol. *55*, 4357–4367. https://doi.org/10.1021/acs.est.0c07465.

35. Li, Y., Shen, J., Zhao, B., Cai, R., Wang, S., Gao, Y., Shrivastava, M., Gao, D., Zheng, J., Kulmala, M., and Jiang, J. (2023). A dynamic parameterization of sulfuric acid–dimethylamine nucleation and its application in three-dimensional modeling. Atmos. Chem. Phys. *23*, 8789–8804. https://doi.org/10.5194/acp-23-8789-2023.

36. Martin, S.T., Artaxo, P., Machado, L.A.T., Manzi, A.O., Souza, R.A.F., Schumacher, C., Wang, J., Andreae, M.O., Barbosa, H.M.J., Fan, J., et al. (2016). Introduction: Observations and Modeling of the Green Ocean Amazon (GoAmazon2014/5). Atmos. Chem. Phys. *16*, 4785–4797. https://doi.org/10.5194/acp-16-4785-2016.

37. Andreae, M.O., Afchine, A., Albrecht, R., Holanda, B.A., Artaxo, P., Barbosa, H.M.J., Borrmann, S., Cecchini, M.A., Costa, A., Dollner, M., et al. (2018). Aerosol characteristics and particle production in the upper troposphere over the Amazon Basin. Atmos. Chem. Phys. *18*, 921–961. https://doi.org/10.5194/acp-18-921-2018.

38. Fan, J., Zhang, Y., Li, Z., Hu, J., and Rosenfeld, D. (2020). Urbanization-induced land and aerosol impacts on sea-breeze circulation and convective precipitation. Atmos. Chem. Phys. *20*, 14163–14182. https://doi.org/10.5194/acp-20-14163-2020.

39. Khain, A., Pokrovsky, A., Pinsky, M., Seifert, A., and Phillips, V. (2004). Simulation of effects of atmospheric aerosols on deep turbulent convective clouds using a spectral microphysics mixed-phase cumulus cloud model. Part I: Model description and possible applications. J. Atmos. Sci. *61*, 2963–2982. https://doi.org/10.1175/jas-3350.1.

40. Wimmer, D., Buenrostro Mazon, S., Manninen, H.E., Kangasluoma, J., Franchin, A., Nieminen, T., Backman, J., Wang, J., Kuang, C., Krejci, R., et al. (2018). Ground-based observation of clusters and nucleation-mode particles in the Amazon. Atmos. Chem. Phys. *18*, 13245–13264. https://doi.org/10.5194/acp-18-13245-2018.

41. Mao, J., Yu, F., Zhang, Y., An, J., Wang, L., Zheng, J., Yao, L., Luo, G., Ma, W., Yu, Q., et al. (2018). High-resolution modeling of gaseous methylamines over a polluted region in China: source-dependent emissions and implications of spatial variations. Atmos. Chem. Phys. *18*, 7933–7950. https://doi.org/10.5194/acp-18-7933-2018.

42. He, Y., Lambe, A.T., Seinfeld, J.H., Cappa, C.D., Pierce, J.R., and Jathar, S.H. (2022). Process-Level Modeling Can Simultaneously Explain Secondary Organic Aerosol Evolution in Chambers and Flow Reactors. Environ. Sci. Technol. *56*, 6262–6273. https://doi.org/10.1021/acs.est.1c08520.

43. Rissanen, M. (2021). Anthropogenic Volatile Organic Compound (AVOC) Autoxidation as a Source of Highly Oxygenated Organic Molecules (HOM). J. Phys. Chem. A *125*, 9027–9039. https://doi.org/10.1021/acs.jpca.1c06465.

44. Tang, S., Xie, S., Zhang, Y., Zhang, M., Schumacher, C., Upton, H., Jensen, M.P., Johnson, K.L., Wang, M., Ahlgrimm, M., et al. (2016). Large-scale vertical velocity, diabatic heating and drying profiles associated with seasonal and diurnal variations of convective systems observed in the GoAmazon2014/5 experiment. Atmos. Chem. Phys. *16*, 14249–14264. https://doi.org/10.5194/acp-16-14249-2016.

45. Fan, J., Leung, L.R., Rosenfeld, D., Chen, Q., Li, Z., Zhang, J., and Yan, H. (2013). Microphysical effects determine macrophysical response for aerosol impacts on deep convective clouds. Proc. Natl. Acad. Sci. USA *110*, E4581–E4590. https://doi.org/10.1073/pnas.1316830110.

46. Holanda, B.A., Franco, M.A., Walter, D., Artaxo, P., Carbone, S., Cheng, Y., Chowdhury, S., Ditas, F., Gysel-Beer, M., Klimach, T., et al. (2023). African biomass burning affects aerosol cycling over the Amazon. Commun. Earth Environ. *4*, 154. https://doi.org/10.1038/s43247-023-00795-5.

47. Shilling, J.E., Pekour, M.S., Fortner, E.C., Artaxo, P., de Sá, S., Hubbe, J.M., Longo, K.M., Machado, L.A.T., Martin, S.T., Springston, S.R., et al. (2018). Aircraft observations of the chemical composition and aging of aerosol in the Manaus urban plume during GoAmazon 2014/5. Atmos. Chem. Phys. *18*, 10773–10797. https://doi.org/10.5194/acp-18-10773-2018.

48. Fast, J.D., Gustafson, W.I., Easter, R.C., Zaveri, R.A., Barnard, J.C., Chapman, E.G., Grell, G.A., and Peckham, S.E. (2006). Evolution of ozone, particulates, and aerosol direct radiative forcing in the vicinity of Houston using a fully coupled meteorology-chemistry-aerosol model. J. Geophys. Res. *111*, D21305. https://doi.org/10.1029/2005jd006721.

49. Grell, G.A., Peckham, S.E., Schmitz, R., McKeen, S.A., Frost, G., Skamarock, W.C., and Eder, B. (2005). Fully coupled "online" chemistry within the WRF model. Atmos. Environ. *39*, 6957–6975.

50. Saha, S., Moorthi, S., Pan, H.L., Wu, X., Wang, J., Nadiga, S., Tripp, P., Kistler, R., Woollen, J., Behringer, D., et al. (2010). THE NCEP CLIMATE FORECAST SYSTEM REANALYSIS. Bull. Am. Meteorol. Soc. *91*, 1015–1058. https://doi.org/10.1175/2010bams3001.1.

51. Hu, Z., Zhao, C., Huang, J., Leung, L.R., Qian, Y., Yu, H., Huang, L., and Kalashnikova, O.V. (2016). Trans-Pacific transport and evolution of aerosols: evaluation of quasi-global WRF-Chem simulation with multiple observations. Geosci. Model Dev. (GMD) *9*, 1725–1746. https://doi.org/10.5194/gmd-9-1725-2016.

52. Zaveri, R.A., Easter, R.C., Fast, J.D., and Peters, L.K. (2008). Model for Simulating Aerosol Interactions and Chemistry (MOSAIC). J. Geophys. Res. *113*, D13204. https://doi.org/10.1029/2007JD008782.

53. Zaveri, R.A., Easter, R.C., Shilling, J.E., and Seinfeld, J.H. (2014). Modeling kinetic partitioning of secondary organic aerosol and size distribution dynamics: representing effects of volatility, phase state, and particle-phase reaction. Atmos. Chem. Phys. *14*, 5153–5181. https://doi.org/10.5194/acp-14-5153-2014.

54. Rasool, Q.Z., Shrivastava, M., Octaviani, M., Zhao, B., Gaudet, B., and Liu, Y. (2021). Modeling Volatility-Based Aerosol Phase State Predictions in the

Amazon Rainforest. ACS Earth Space Chem. *5*, 2910–2924. https://doi.org/10.1021/acsearthspacechem.1c00255.

55. Zhao, C., Huang, M., Fast, J.D., Berg, L.K., Qian, Y., Guenther, A., Gu, D., Shrivastava, M., Liu, Y., Walters, S., et al. (2016). Sensitivity of biogenic volatile organic compounds to land surface parameterizations and vegetation distributions in California. Geosci. Model Dev. (GMD) *9*, 1959–1976. https://doi.org/10.5194/gmd-9-1959-2016.
56. Shrivastava, M., Andreae, M.O., Artaxo, P., Barbosa, H.M.J., Berg, L.K., Brito, J., Ching, J., Easter, R.C., Fan, J., Fast, J.D., et al. (2019). Urban pollution greatly enhances formation of natural aerosols over the Amazon rainforest. Nat. Commun. *10*, 1046. https://doi.org/10.1038/s41467-019-08909-4.
57. Song, C., Zaveri, R.A., Alexander, M.L., Thornton, J.A., Madronich, S., Ortega, J.V., Zelenyuk, A., Yu, X.Y., Laskin, A., and Maughan, D.A. (2007). Effect of hydrophobic primary organic aerosols on secondary organic aerosol formation from ozonolysis of α-pinene. Geophys. Res. Lett. *34*, L20803. https://doi.org/10.1029/2007gl030720.
58. Vaden, T.D., Song, C., Zaveri, R.A., Imre, D., and Zelenyuk, A. (2010). Morphology of mixed primary and secondary organic particles and the adsorption of spectator organic gases during aerosol formation. Proc. Natl. Acad. Sci. USA *107*, 6658–6663. https://doi.org/10.1073/pnas.0911206107.
59. Hodshire, A.L., Akherati, A., Alvarado, M.J., Brown-Steiner, B., Jathar, S.H., Jimenez, J.L., Kreidenweis, S.M., Lonsdale, C.R., Onasch, T.B., Ortega, A.M., and Pierce, J.R. (2019). Aging Effects on Biomass Burning Aerosol Mass and Composition: A Critical Review of Field and Laboratory Studies. Environ. Sci. Technol. *53*, 10007–10022. https://doi.org/10.1021/acs.est.9b02588.
60. Freitas, S.R., Longo, K.M., Chatfield, R., Latham, D., Silva Dias, M.A.F., Andreae, M.O., Prins, E., Santos, J.C., Gielow, R., and Carvalho, J.A. (2007). Including the sub-grid scale plume rise of vegetation fires in low resolution atmospheric transport models. Atmos. Chem. Phys. *7*, 3385–3398. https://doi.org/10.5194/acp-7-3385-2007.
61. Zhang, Y., Fan, J., Logan, T., Li, Z., and Homeyer, C.R. (2019). Wildfire Impact on Environmental Thermodynamics and Severe Convective Storms. Geophys. Res. Lett. *46*, 10082–10093. https://doi.org/10.1029/2019GL084534.
62. Akherati, A., He, Y., Coggon, M.M., Koss, A.R., Hodshire, A.L., Sekimoto, K., Warneke, C., de Gouw, J., Yee, L., Seinfeld, J.H., et al. (2020). Oxygenated Aromatic Compounds are Important Precursors of Secondary Organic Aerosol in Biomass-Burning Emissions. Environ. Sci. Technol. *54*, 8568–8579. https://doi.org/10.1021/acs.est.0c01345.
63. Majluf, F.Y., Krechmer, J.E., Daube, C., Knighton, W.B., Dyroff, C., Lambe, A.T., Fortner, E.C., Yacovitch, T.I., Roscioli, J.R., Herndon, S.C., et al. (2022). Mobile Near-Field Measurements of Biomass Burning Volatile Organic Compounds: Emission Ratios and Factor Analysis. Environ. Sci. Technol. Lett. *9*, 383–390. https://doi.org/10.1021/acs.estlett.2c00194.
64. Permar, W., Wang, Q., Selimovic, V., Wielgasz, C., Yokelson, R.J., Hornbrook, R.S., Hills, A.J., Apel, E.C., Ku, I.-T., Zhou, Y., et al. (2021). Emissions of Trace Organic Gases From Western U.S. Wildfires Based on WE-CAN Aircraft Measurements. JGR. Atmospheres *126*, e2020JD033838. https://doi.org/10.1029/2020JD033838.
65. Darmenov, A.S., and da Silva, A. (2015). The Quick Fire Emissions Dataset (QFED): Documentation of Versions 2.1, 2.2 and 2.4. In Technical Report Series on Global Modeling and Data Assimilation (NASA Goddard Space Flight Center).
66. Pierce, J.R., and Adams, P.J. (2009). A Computationally Efficient Aerosol Nucleation/Condensation Method: Pseudo-Steady-State Sulfuric Acid. Aerosol. Sci. Technol. *43*, 216–226. Pii 906615196. https://doi.org/10.1080/02786820802587896.
67. Riccobono, F., Schobesberger, S., Scott, C.E., Dommen, J., Ortega, I.K., Rondo, L., Almeida, J., Amorim, A., Bianchi, F., Breitenlechner, M., et al. (2014). Oxidation Products of Biogenic Emissions Contribute to Nucleation of Atmospheric Particles. Science *344*, 717–721. https://doi.org/10.1126/science.1243527.
68. Li, Y., Shen, J., Zhao, B., Cai, R., Wang, S., Gao, Y., Shrivastava, M., Gao, D., Zheng, J., Kulmala, M., and Jiang, J. (2023). A parameterization of sulfuric acid-dimethylamine nucleation and its application in three-dimensional modeling. Atmos. Chem. Phys. Discuss. *2023*, 1–22. https://doi.org/10.5194/acp-2023-15.
69. Fan, J., Wang, Y., Rosenfeld, D., and Liu, X. (2016). Review of Aerosol-Cloud Interactions: Mechanisms, Significance, and Challenges. J. Atmos. Sci. *73*, 4221–4252. https://doi.org/10.1175/jas-d-16-0037.1.
70. Khain, A.P., Beheng, K.D., Heymsfield, A., Korolev, A., Krichak, S.O., Levin, Z., Pinsky, M., Phillips, V., Prabhakaran, T., Teller, A., et al. (2015). Representation of microphysical processes in cloud-resolving models: Spectral (bin) microphysics versus bulk parameterization. Rev. Geophys. *53*, 247–322. https://doi.org/10.1002/2014RG000468.
71. Zhang, Y., Fan, J., Li, Z., and Rosenfeld, D. (2021). Impacts of cloud microphysics parameterizations on simulated aerosol–cloud interactions for deep convective clouds over Houston. Atmos. Chem. Phys. *21*, 2363–2381. https://doi.org/10.5194/acp-21-2363-2021.
72. Gevaerd, R., and Freitas, S.R. (2006). Estimativa operacional da umidade do solo para iniciação de modelos de previsão numérica da atmosfera. Parte I: Descrição da metodologia e validação. Revista Brasileira de Meteorologia *21*, 1–15.
73. Beck, V., Gerbig, C., Koch, T., Bela, M.M., Longo, K.M., Freitas, S.R., Kaplan, J.O., Prigent, C., Bergamaschi, P., and Heimann, M. (2013). WRF-Chem simulations in the Amazon region during wet and dry season transitions: evaluation of methane models and wetland inundation maps. Atmos. Chem. Phys. *13*, 7961–7982. https://doi.org/10.5194/acp-13-7961-2013.